Chemical Methodologies 10(2026) 75-111

Chemical Methodologies

Journal homepage: http://chemmethod.com

Original Article

# An Innovative Method for Complex Processing of Black Shale Ores to Produce Uranium, Vanadium, Molybdenum, and Rare Earth Concentrates

**Tatyana Chepushtanova[1], Sultan Yulussov[1], Omirserik Baigenzhenov[1,*], Alibek Khabiev[1], Kanay Rysbekov[1], Norlin Nosbi[2], M. Barmenshinova[1], Nur Nabihah Yusof[3], Yerik Merkibaev[1], Ahmad Hosseini-Bandegharaei[4,5,6]**

[1]*Department of Metallurgy and Mineral Processing, Satbayev University, Almaty 050013, Kazakhstan*
[2]*Mechanical Engineering Department, Universiti Teknologi Petronas, Seri Iskandar, Perak, 32610, Malaysia*
[3]*School of Physics, Universiti Sains Malaysia, 11800 USM, Penang, Malaysia*
[4]*Faculty of Chemistry, Semnan University, Semnan, Iran*
[5]*Department of Sustainable Engineering, Saveetha School of Engineering, SIMATS, Chennai 602105, Tamil Nadu, India*
[6]*Centre of Research Impact and Outcome, Chitkara University, Rajpura 140401, Punjab, India*

**ARTICLEINFO**

**Article history**
Submitted: 2025-07-16
Revised: 2025-08-16
Accepted: 2025-09-10
ID: CHEMM-2507-1988

**DOI**: 10.48309/chemm.2026.535012.1988

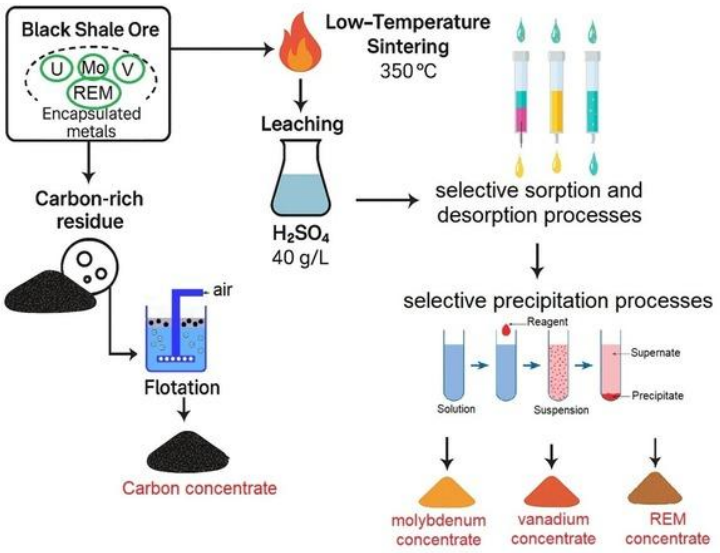
**KEYWORDS**
Black shale ore
Sintering
Leaching
Concentrate
REM
Sorption
Concentrate

**ABSTRACT**

The current study provides a new leaching method for extracting valuable metals, such as uranium, vanadium, molybdenum, and rare earth metals (REMs), from black shale ores. Initial characterization indicated that these metals are encapsulated in hard "carbon-silica shells," presenting severe extraction challenges. A novel low-temperature sintering process is considered in this work with ammonium hydrosulfate at 350 °C for 60 minutes, much lower than the conventional process of over 800 °C. The devised treatment effectively ruptures the protective shell, converting metal constituents into soluble forms. Subsequent leaching yielded good recovery rates: uranium (93.3%), vanadium (81.7%), molybdenum (82.2%), and REMs (78.3%). Thermogravimetric analysis revealed the stepwise decomposition mechanism and emission profiles upon sintering. The leaching parameters (solid-liquid ratio, temperature, time, and solution concentration) were optimized for maximum metal recovery, along with selective sorption conditions (pH, redox potential, and duration) and desorption variables. Additionally, the cost-effective production routes for vanadium concentrate were specified as ammonium metavanadate, molybdenum concentrate as calcium molybdate and REM concentrate as carbonates, instead of depending on high-pressure or high-temperature processes. Solid residue carbon flotation enrichment was accompanied by a recovery yield of 89.0% by weight of carbon, enabling enhanced utilization of the entire resource. Altogether, the adopted approaches offer a closed-loop, energy-saving pathway to the efficient recovery of the rare and essential metals from the black shale ore.

* Corresponding author: Omirserik Baigenzhenov
E-mail: obaigenzhenov@gmail.com
© 2026 by Sami Publishing Company
This is an open access article under the CC BY license

**GRAPHICAL ABSTRACT**




## Introduction

Black shale ores are fine-grained sedimentary rocks that have a high organic carbon content [1,2] and are formed in anoxic depositional environments that favour preservation of organic matter and enrichment of some metals. The geochemical conditions favour the concentration of economically imperative elements, such as vanadium, molybdenum, uranium, and rare earth elements, in the matrix of shale. In response to ever-decreasing conventional ore reserves, black shale ores have gained importance as potential substitute resources with exploitable concentrations of refractory, radioactive, and rare earth metals amenable to integrated extraction schemes [3]. Hence, these deposits present a valuable frontier for the exploitation of strategic metals essential for sophisticated technological applications.

A wide variety of processing techniques has been studied for treating black shale ores, and hydrometallurgical treatment-that is, acid leaching at atmospheric as well as autoclave pressures-remains most prevalent in literature [4,5]. Additionally, initial pyrometallurgical treatment, *i.e.,* sintering, is commonly employed to enhance solubility of the valuable metals prior to leaching. Notably, recent advances have introduced a new two-stage fluidized bed calcination process to optimize the recovery of certain elements, such as vanadium. In this process, the initial stage is conducted at 650 °C for 60 minutes, which attains a considerable 95.89% reduction in carbon content and promotes the decomposition of kaolinite and dolomite. The second stage, performed at 950 °C for 75 minutes, results in dehydroxylation of vanadium minerals bearing vanadium and thus destabilizing the mineral matrix and facilitating the easier extraction during subsequent leaching. This technique has yielded a recovery rate of vanadium from leachates of 68.54%-or a 39.28% increase over untreated ore-as well as a 13.54% increase over single-stage roasting with the addition of NaCl, highlighting the efficiency of combined thermal pretreatment in advancing extraction of key metals from black shale matrices [6]. While hydrometallurgical technologies - particularly acid leaching - have long been favored for the extraction of valuable metals from complex mineral matrices due to their operational versatility, scalability, and adaptability to diverse ore types, their overall efficiency and selectivity remain critically dependent on the extent of prior mineralogical modification of the feed material. In many refractory black shale ores, the limited leachability of target metals is primarily a consequence of their encapsulation within silicate lattices or close association with resistant gangue minerals. Such structural confinement

restricts reagent access to reactive sites, thereby slowing dissolution kinetics and reducing recovery rates. Consequently, pyrometallurgical or thermochemical pretreatment is frequently required to induce lattice breakdown, liberate metal-bearing phases, and improve the performance of subsequent hydrometallurgical processing [7].

Recent advances in thermochemical treatment have increasingly focused on sustainable, low-energy strategies such as low-temperature activation, selective roasting, and controlled-atmosphere processing. For example, Zhou *et al.* [8] demonstrated that suspension oxidation roasting markedly enhances vanadium extraction from muscovite-type black shale by deconstructing the mineral lattice and improving reagent access. Microwave-assisted roasting further reduces energy inputs and process duration, as shown by Lode *et al.* [9], with significant release of REMs, V, Ni, and Li under milder conditions. The concept of "selective roasting" has been highlighted in metastructural metallurgy research, emphasizing minimized volatilization losses while preserving valuable co-products (Raabe.). Additionally, Aleksandrova *et al.* [10] applied low-temperature, energy-mediated treatments to unlock noble and rare metal structures in carbonaceous ores, illustrating the effectiveness of targeted activation in complex matrices.

The pronounced variability of black shale ores is well documented across global deposits. In South China, Lower Cambrian black shales are enriched in vanadium, with average contents of approximately 0.65 wt% V and local maxima exceeding 1.19 wt%, alongside significant Zn, Cu, U, and Ni. In western Hunan, molybdenum concentrations may reach 2.2–4.6 wt%, with nickel contents of 1.1–1.7 wt% in the richest horizons [11]. Scandinavia's Cambrian Alum Shale is a distinct metallogenic type, notable for uranium levels of 100–300 ppm, combined Mo and V enrichment, and exceptionally high total organic matter contents (up to 28 wt%), which strongly influence metal partitioning and extraction behavior. In the United States, Paleozoic and Mesozoic black shales - such as the Chattanooga Shale and the Houy Formation - contain a broad suite of critical and base metals, including U, Cu, Ni, V, Mo, Co, Tl, Pb, and Zn, with these elements typically hosted in organic matter and finely disseminated pyrite [12].

These examples make clear that "black shale ore" does not represent a single geochemical category but rather a spectrum of metallogenic systems, ranging from V–Mo–Ni-dominant assemblages (*e.g.,* South China, Karatau) to U-rich organic shales (*e.g.,* Alum, Chattanooga). This diversity has direct implications for extractive metallurgy: the design of an effective processing strategy - whether based on thermal activation, oxidative or reductive roasting, optimized oxidant systems, or specialized complexing agents - must be guided by a detailed understanding of the dominant metals, their mineralogical and textural contexts, and the specific grade distribution of the deposit in question. Transferring processing schemes across geologically dissimilar deposits without such adaptation often results in suboptimal recoveries, excessive reagent consumption, or unnecessary energy expenditure.

Numerous studies have focused on leaching of metals from black shale ores with acid mixtures [13]. For instance, one study investigated vanadium recovery from Guizhou black shale in China, and it found that vanadium mainly exists in oxide and mica mineral phases. The researchers conducted a systematic study on the effect of key leaching parameters-*i.e.,* reaction time, sulfuric acid ($H_2SO_4$) and hydrofluoric acid (HF) concentration, sodium hypochlorite (NaClO) dosage, temperature, and liquid-to-solid ratio-on vanadium recovery [14]. Under optimal conditions, using a leaching time of 6 hours, 87.5 g/L $H_2SO_4$, 15 g/L HF, and the addition of 1 g/L NaClO at 3 hours with a temperature of 95 °C and a liquid-to-solid ratio of 4 mL/g, vanadium extraction reached a maximum of 86%. HF was found to be absolutely crucial in the leaching process of refractory mineral matrices for successful breakdown. Notably, reducing the leaching temperature from 150 °C to 95 °C caused the optimized single-stage process to experience quite a moderate 4% loss in vanadium recovery compared to a conventional two-stage

countercurrent process, thereby demonstrating the effectiveness of the sulfuric and hydrofluoric acid system at lower temperatures [8]. The chemical complexity of black shale ores often requires multireagent systems to achieve satisfactory recovery rates. The synergistic use of strong acids with fluoride, for example, has been shown to substantially enhance vanadium extraction efficiency, with leaching outcomes heavily dependent on parameters such as acid concentration, fluoride dose, temperature, and time [15]. The addition of oxidizing agents alongside fluorinating aids can further improve leaching performance by disrupting refractory mineral structures, such as garnet, leading to high extraction efficiency (up to ~94.9 %) while reducing acid consumption [16].

Recent studies on the autoclaving leaching of black shale ores have revealed its superior performance in leaching valuable metals under high pressure and high temperature conditions, which greatly accelerates the leaching kinetics compared to the conventional method [14,17]. For example, leaching tests on Guizhou deposit ore containing 3.2% $V_2O_5$, 52.8% $SiO_2$, and 16.1% $Al_2O_3$ indicated that the optimum single-stage leaching-performed at 150 °C for 3 hours with 25% sulfuric acid and a liquid-to-solid ratio of 1.2 mL/g-achieved vanadium recoveries of approximately 77%. Based on this purpose, a two-stage counter-current leaching method was developed, setting parameters such as reaction time, acid concentration, temperature, liquid-to-solid ratio, and $FeSO_4$ addition, and which increased the extraction efficiency of vanadium to well over 90% [17]. However, consideration of the optimal ore treatment method must extend significantly beyond extraction efficiency to incorporate some measure of reagent consumption, material and equipment design necessity, production scale, integration, and performance at downstream stages in the process. This systemic, integrated approach guarantees both the cost-effectiveness and higher overall productivity and utilization of resources in the extraction operation. Although high-pressure, high-temperature autoclave leaching can achieve rapid dissolution kinetics, the operational and capital costs, coupled with stringent safety requirements, limit its broad applicability - especially in decentralized or resource-constrained operations [18]. From a system engineering perspective, process selection should integrate not only extraction yield, but also downstream separation efficiency, water and reagent recycling potential, and overall carbon footprint. This holistic framework aligns with the principles of sustainable metallurgy, where process intensification is balanced with environmental stewardship and lifecycle resource efficiency.

Black shales are rich in ores of not only vanadium but also large quantities of uranium, molybdenum, and REMs [19-21]. All these associated metals are also leached in the hydrometallurgical extraction of vanadium. All current processes lean toward vanadium to detriment of the overall recovery of these other valuable constituents. Selective application of extraction methods focused on uranium, molybdenum, and REMs provides an opportunity to improve the economic feasibility and broaden the technology scope for processing black shales . Adopting a review of the literature, one can grasp that extensive research and development efforts have been devoted to processing black shale ores, testifying to the complexity and challenges of extracting valuable metals from these refractory materials.

Maximizing the value proposition of black shale exploitation requires a paradigm shift from single-metal recovery toward multi-element beneficiation, ensuring the economic viability of processing low-grade and refractory resources. Advances in selective sorption, ion exchange, and solvent extraction technologies now allow for precise separation of closely associated metals, such as Mo and V, or U and REEs, even in complex leachates. By integrating these separation steps into an optimized flowsheet, it becomes feasible to recover a diversified suite of high-purity products while reducing waste volumes and improving overall economics. In this article, a detailed mineralogical and chemical characterization of black shale ores is first presented, emphasizing the challenges posed by

the refractory "carbon-silica shell." This is followed by an in-depth description of the novel low-temperature ammonium hydrosulfate sintering process and its thermodynamic basis. Subsequently, the optimization of leaching parameters and the selective sorption, as well as desorption techniques employed for individual valuable metals are discussed. Finally, the study concludes with the evaluation of product recovery, carbon flotation enrichment, and overall process efficiency, highlighting the sustainability and industrial applicability of the proposed integrated technology.

## Experimental

*Materials and Analysis*

The object of the study was representative samples of black shale ores from the "Big Karatau" deposit. For the analysis of initial samples and experimental products, X-ray fluorescence (Olympus Vanta C Series XRF Analyzer), X-ray phase (D8 Advance diffractometer (BRUKER)), and thermographic methods (STA 409, 449 PC/PG - NETZSCH) were used. Elemental composition analyses of minerals (microinclusions) and photography in various types of radiation were performed using an energy-dispersive spectrometer INCA ENERGY from OXFORD INSTRUMENTS, installed on the electron probe microanalyzer SUPERPROBE –733 at an accelerating voltage of 25 kV and a probe current of 25 nA. Infrared spectroscopic analysis data were obtained using the FTIR spectrometer Thermo Nicolet Avatar 370 FTIR Spectrometer, 2002, in the range of 400-3,600 $cm^{-1}$.

All necessary sample weighing during the work was carried out on analytical balances RA214C (Ohaus-Pioneer) with an accuracy of 0.0005 g. Before the start of pyrometallurgical and hydrometallurgical processes, the initial ore was pre-ground to a particle size of -0.074 mm. To ensure the reliability of the obtained results, samples were analyzed three times using the X-ray fluorescence analyzer, and the averaged result of all analyses was reported in Table 1.

**Table 1:** The composition of the black shale ores

| Component | Content, % | Component | Content, % | Component | Content, % |
|---|---|---|---|---|---|
| $Al_2O_3$ | 3.792 | S | 0.807 | $U_3O_8$ | 0.027 |
| $Fe_2O_3$ | 2.077 | Sr | 0.049 | $ZrO_2$ | 0.010 |
| $K_2O$ | 1.161 | C | 14.72 | $CeO_2$ | 0.011 |
| CaO | 0.383 | Cr | 0.042 | $Nd_2O_3$ | 0.01 |
| $SiO_2$ | 72.35 | $SO_3$ | 1.362 | $SeO_2$ | 0.007 |
| MgO | 0.292 | Cl | 0.081 | $Tb_4O_7$ | 0.005 |
| $Na_2O$ | 0.067 | $WO_3$ | 0.035 | $Rb_2O$ | 0.004 |
| $TiO_2$ | 0.119 | Cu | 0.041 | $Tl_2O_3$ | 0.003 |
| $P_2O_5$ | 1.155 | Mo | 0.042 | $PtO_2$ | 0.003 |
| Ba | 0.776 | As | 0.009 | REM | 0.09 |
| V | 0.715 | Ni | 0.008 | Co | 0.008 |

Based on the analysis results, the ore not only contains vanadium, but also valuable metals such as uranium, molybdenum, and rare earth metals (REMs). Processing these metals concurrently with vanadium allows for their comprehensive extraction, thereby broadening the portfolio of commercially viable products. To assess the elemental composition of minerals, including microinclusions, comprehensive samples of the ore material were prepared. These samples encompass grains from various regions with a high concentration of rare and rare-earth metals. Figure 1 illustrates these grains, which appear as bright spots contrasted with darker surrounding areas.

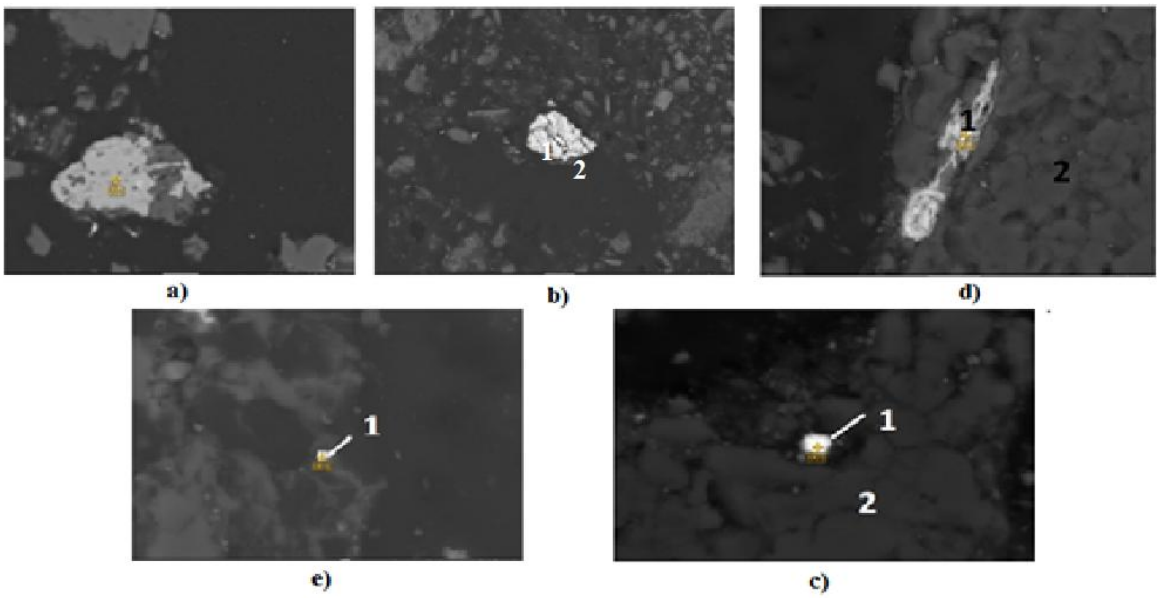



**Figure 1:** Microphotographs of the initial black shale ore: a) Rutile containing vanadium; b) 1 - Rare Earth Metals (REM) phosphates, 2 – "carbon-silica shell"; d) Uraninite, 2 – "carbon-silica shell"; e) Patronite, 2 – "carbon-silica shell"; c) 1 - Molybdenite, 2 – "carbon-silica shell"

Figure 1 displays a series of representative reflected-light microphotographs of the initial black shale ore, revealing the mineralogical heterogeneity, phase associations, and the pervasive encapsulation of valuable metals within the "carbon-silica shell". In Figure 1a, rutile ($TiO_2$) containing finely disseminated vanadium occurs as high-reflectance, light-gray to white grains exhibiting subhedral to anhedral crystal habits, set within a darker siliceous–carbonaceous matrix. Figure 1b illustrates rare earth metal (REM) phosphates (label 1) in the form of discrete, angular to rounded bright inclusions, surrounded by a distinct "carbon-silica shell" (label 2), which appears as a medium- to dark-gray rim exhibiting uniform thickness. In Figure 1c, molybdenite ($MoS_2$) (label 1) is identified by its characteristic silvery metallic luster and platy, lamellar morphology, also encapsulated by the carbon–silica shell (label 2), which imparts a distinct optical contrast under reflected light. Figure 1d presents uraninite ($UO_2$) grains as high-relief, isotropic, light-gray to white phases with sharply defined boundaries, enveloped by the carbon-silica shell (label 2), indicative of syngenetic encapsulation during sedimentary diagenesis. Figure 1e shows patronite ($VS_4$) (label 1) occurring in fine-grained aggregates with irregular morphology, likewise surrounded by the carbon–silica shell (label 2). Across all microphotographs, the carbon–silica shell exhibits a consistent optical signature - a subdued reflectance and uniform tone relative to the enclosed mineral phase - reflecting its composite nature of amorphous to microcrystalline silica intimately mixed with carbonaceous matter. This shell acts as a robust physical–chemical barrier, severely limiting reagent access and dissolution kinetics during direct leaching. The observed mineral - shell associations underscore the refractory character of the ore and substantiate the necessity for pretreatment strategies, such as low-temperature ammonium hydrosulfate sintering, to induce shell breakdown, liberate the metal-bearing phases, and improve subsequent hydrometallurgical recovery efficiency.

The XRD analysis of the black shale sample identified a mineralogical composition that predominantly consists of aluminosilicate minerals, including anorthite, muscovite, paravollastonite, mullite, kaolinite, roscoelite, muscovite and phengite. In addition, the sample contained sulfide minerals such as pyrite, sulvanite, patronite, and molybdenite, as well as oxide minerals such as quartz, aluminum oxide,

and dolomite. Based on the data, rare earth metals (REMs) in black shale ore are found in various minerals and are encapsulated in a carbon-silica matrix (carbon-silica shell). Therefore, when processing the raw material to extract rare and rare earth metals, it is necessary to consider the properties of the minerals that surround and encapsulate the valuable metals and find ways to break down the "carbon-silica shell".

*Thermodynamic Patterns of Studied Processes*

Thermodynamic calculations play an imperative role in various fields of science and engineering, providing a deep understanding of the processes occurring in the studied systems [22]. Such calculations allow for predicting behaviors of systems under different conditions, which is especially important in chemical reactions where it is essential to know which ones occur spontaneously and which ones require external interventions. An important aspect of thermodynamics is determining the equilibrium position of a system, which grants an understanding of the long-term state of the system and the factors that can influence this state. Thermodynamic calculations help researchers optimize conditions for various processes [23], which can indicate selecting the optimal temperature and pressure to maximize production yield or minimize energy expenses. In today's world, where energy resources are becoming increasingly valuable, thermodynamic calculations enable the development of more efficient systems, improving existing technologies and creating new, more energy-efficient solutions.

As shown by the physicochemical analyses of the original black shale ores, the main components of the ore are aluminosilicate, silicate, and carbonate minerals, which form the main matrix of the ore and create a "carbon-silica shell" that hinders the extraction of valuable components. To preliminarily assess the method, thermodynamic calculations of the sintering process were performed based on the proposed reactions. The calculations were implemented by exploiting the HSC Chemistry 5.11 software (developed by Outokumpu). The calculations were conducted in the temperature range of 150 to 350 ℃.

*Thermodynamic Patterns of the Sintering Process*

Sintering black shale ore with ammonium hydrosulfate aims to break down the "carbon-silica shell" by converting silica and carbon into a stable crystalline structure, and metals into a water-soluble form. The decomposition of ammonium hydrosulfate in the temperature range of 150 to 350 ℃ proceeds quite actively, forming ammonium sulfate and sulfuric acid, while the release of ammonia, carbon dioxide, and water begins above 350 ℃. The obtained data indicate that ammonium hydrosulfate forms a melt at temperatures from 150 to 350 ℃, and decomposes into ammonia and carbon dioxide above 350 ℃.

Thermodynamic calculations of the sintering process of ammonium hydrosulfate with rock-forming minerals are presented in Table 2. The reaction of anorthite ($2CaO{\cdot}Al_2O_3{\cdot}SiO_2$), muscovite ($K_2O{\cdot}Al_2O_3{\cdot}2SiO_2$), dolomite ($CaMg(CO_3)_2$), and parawollastonite ($CaSiO_3$) with ammonium hydrosulfate and its decomposition products at temperatures of 100-350 ℃ proceeds quite actively, as there is a change in Gibbs free energy.

The decomposition of rock-forming aluminosilicate, silicate, and carbonate minerals upon heating is accompanied by the formation of metal oxides and the release of crystallization water. Simultaneously, ammonium hydrosulfate decomposes into ammonium sulfate and sulfuric acid, with partial release of $CO_2$ and $NH_3$. As a result of the interaction between metal oxides and ammonium hydrosulfate, water-soluble sulfate complexes of aluminum, calcium, potassium, and magnesium are formed. Additionally, thermodynamic calculations of the sintering process indicate that the ore minerals patronite, uraninite, and REM phosphate actively interact with ammonium hydrosulfate and its decomposition products, forming water-soluble compounds (Table 3).

**Table 2:** Thermodynamic calculations of the decomposition of mineral components in the "carbon-silica shell" with ammonium hydrosulfate

| Name of the mineral | Characteristics | Temperature (°C) | | | | |
|---|---|---|---|---|---|---|
| | | 150 | 200 | 250 | 300 | 350 |
| Anorthite | $CaO{\cdot}Al_2O_3{\cdot}SiO_2 + 4NH_4HSO_4 \rightarrow CaSO_4 + Al_2(SO_4)_3 + SiO_2 + 4H_2O + 4NH_3\uparrow$ | | | | | |
| | ΔH | 287.92 | 288.21 | 287.02 | 285.12 | 284.42 |
| | ΔS | 1070.82 | 1071.50 | 1069.12 | 1065.68 | 1064.48 |
| | ΔG | -165.19 | -218.76 | -272.29 | -325.66 | -378.91 |
| Muscovite | $K_2O{\cdot}Al_2O_3{\cdot}SiO_2 + 4NH_4HSO_4 \rightarrow Al_2(SO_4)_3 + K_2SO_4 + 2SiO_2 + 4H_2O + 4NH_3\uparrow$ | | | | | |
| | ΔH | 293.28 | 292.72 | 290.49 | 287.49 | 285.74 |
| | ΔS | 1054.37 | 1053.15 | 1048.69 | 1043.23 | 1040.28 |
| | ΔG | -152.87 | -205.58 | -258.12 | -310.43 | -362.51 |
| Dolomite | $CaMg(CO_3)_2 + 2NH_4HSO_4 \rightarrow CaSO_4 + MgSO_4 + 2CO_2(g) + 2H_2O + 2NH_3\uparrow$ | | | | | |
| | ΔH | 201.13 | 200.67 | 199.44 | 197.85 | 196.84 |
| | ΔS | 879.62 | 878.60 | 876.15 | 873.25 | 871.55 |
| | ΔG | -171.08 | -215.05 | -258.92 | -302.65 | -346.27 |
| Parawollastonite | $CaSiO_3 + NH_4HSO_4 \rightarrow CaSO_4 + SiO_2 + H_2O + NH_3$ | | | | | |
| | ΔH | -19.05 | -19.09 | -19.48 | -20.00 | -20.18 |
| | ΔS | 271.75 | 271.66 | 270.89 | 269.93 | 269.64 |
| | ΔG | -134.04 | -147.63 | -161.19 | -174.71 | -188.2 |
| Mullite | $Al_2Si_2O_7{\cdot}2H_2O + 2NH_4HSO_4 \rightarrow Al_2(SO_4)_3 + 2SiO_2 + 5H_2O + 11NH_3\uparrow$ | | | | | |
| | ΔH | 364.18 | 368.18 | 371.80 | 378.02 | 383.37 |
| | ΔS | 913.92 | 913.92 | 927.39 | 937.76 | 946.03 |
| | ΔG | -67.66 | -113.53 | -159.73 | -206.34 | -253.45 |

**Table 3:** Thermodynamic calculations of the decomposition of ore minerals with ammonium hydrosulfate

| Name of the mineral | Characteristics | Temperatures (°C) | | | | |
|---|---|---|---|---|---|---|
| | | 150 | 200 | 250 | 300 | 350 |
| Patronite | $V_2S_3 + 12NH_4HSO_4 \rightarrow 2VOSO_4 + 13SO_2 + 12H_2O + 12NH_3\uparrow$ | | | | | |
| | ΔH | 2372.03 | 2366.18 | 2355.27 | 2341.97 | 2332.10 |
| | ΔS | 5761.75 | 5748.79 | 5726.95 | 5702.68 | 5686.13 |
| | ΔG | -66.052 | -353.86 | -640.78 | -926.52 | -1211.21 |
| | $VS + 5\,NH_4HSO_4 \rightarrow VOSO_4 + 5\,SO_2 + 5\,H_2O + 5\,NH_3\uparrow$ | | | | | |
| | ΔH | 874.51 | 874.81 | 873.13 | 870.56 | 869.53 |
| | ΔS | 2329.25 | 2329.96 | 2326.60 | 2321.92 | 2320.17 |
| | ΔG | -111.11 | -227.61 | -344.04 | -460.25 | -576.29 |
| Nasturan | $UO_3{\cdot}H_2O + NH_4HSO_4 \rightarrow UO_2SO_4 + 2\,H_2O + NH_3\uparrow$ | | | | | |
| | ΔH | 105.31 | 106.59 | 107.58 | 108.74 | 111.07 |
| | ΔS | 307.84 | 310.69 | 312.68 | 314.80 | 318.69 |
| | ΔG | -24.95 | -40.42 | -56.00 | -71.69 | -87.52 |
| Monazite | $2\,LaPO_4 + 3\,NH_4HSO_4 \rightarrow La_2(SO_4)_3 + 2\,H_3PO_4 + 3\,NH_3\uparrow$ | | | | | |
| | ΔH | 269.54 | 267.39 | 264.04 | 259.54 | 253.93 |
| | ΔS | 777.89 | 773.13 | 766.42 | 758.21 | 748.84 |
| | ΔG | -59.63 | -98.41 | -136.91 | -175.03 | -212.71 |
| | $2LaPO_4 + Al_2(SO_4)_3 \rightarrow La_2(SO_4)_3 + 2AlPO_4$ | | | | | |
| | ΔH | -165.01 | -168.74 | -172.86 | -177.18 | -181.56 |
| | ΔS | 12.56 | 4.25 | -4.03 | -11.91 | -19.25 |
| | ΔG | -170.33 | -170.75 | -170.75 | -170.35 | -169.57 |
| Molybdenite | $MoS_2 + NH_4HSO_4 \rightarrow MoO_3 + 3SO_2\uparrow + H_2O + NH_3\uparrow$ | | | | | |
| | ΔH | -667.2 | -668.3 | -669.6 | -670.4 | -671.5 |
| | ΔS | 342.3 | 340.1 | 337.9 | 336.5 | 334.7 |
| | ΔG | - 829.2 | -846.3 | -863.2 | -880.1 | -896.9 |

The calculation of thermodynamic potentials of phase transformations has established the mechanism of the breakdown of ore and non-ore minerals, which is based on the formation of

water-soluble sulfate complexes of all valuable elements: uranium, vanadium, and rare earth metals, as a result of the interaction of disintegrated metal oxides with ammonium hydrosulfate. Pressure oxidative leaching has also been successfully applied to recover vanadium from calcified stone coal concentrates. Huang *et al.* [24] demonstrated that a two-stage process—initial dilute sulfuric acid dephosphorization followed by pressure acid leaching in an oxygen-enriched environment - can achieve both high vanadium recovery and effective impurity removal. In their study, the roasted concentrate was leached at 200 °C under a total pressure of 2.0 MPa, with an oxygen partial pressure of 0.8 MPa, using 20 % $H_2SO_4$ for 120 minutes. Under these optimized conditions, vanadium recovery reached 92.3 %, while the contents of phosphorus and aluminum in the leach liquor were significantly reduced, facilitating downstream purification. The high temperature and oxygen pressure promoted the breakdown of muscovite and the oxidation of V(IV) to V(V), thereby enhancing dissolution rates. This approach, although requiring autoclave infrastructure, offers a viable route for upgrading low-grade stone coal while minimizing reagent consumption in subsequent separation stages. However, this method entails significantly higher energy consumption. In the case of stone coal, the use of additives such as NaCl (and $Na_2CO_3$ or CaO) has been shown to disrupt vanadium-bearing mica structures, enhancing recovery rates to ~91 % under optimized conditions [25]. In contrast, our thermal treatment regime at 350 °C achieves comparable or superior recovery efficiencies (U ≈ 93 %, V ≈ 82 %, Mo ≈ 82 %, ΣREE ≈ 78 %) with substantially lower energy input. Such an environmentally friendlier, low-temperature activation mechanism aligns with recent sustainable metallurgical strategies [26].

*Research Workflow*

Figure 2 schematically illustrates the integrated technological flowsheet developed and investigated in this work for the recovery of valuable and rare earth metals from black shale ores. The process commences with low-temperature sintering, performed under optimized thermochemical conditions to induce structural transformation of the mineral matrix and convert the target components into a more readily leachable form. Sintering the ore prior to the leaching process enhances both the efficiency and quality of leaching [27]. This technique increases the ore's porosity, facilitating the penetration of the leaching solution and its interaction with valuable components.

Additionally, sintering can remove certain undesirable impurities, thereby improving the final product's quality and reducing the burden on subsequent processing stages. Furthermore, sintering enhances the ore's reactivity, thereby accelerating the leaching process and increasing its overall efficiency. The addition of various salts or acids during sintering can convert valuable ore components into easily acid-soluble forms [28]. The leach solution, containing the dissolved rare and rare earth elements, is subsequently processed through selective sorption recovery using ion-exchange resins. At this stage, critical parameters such as pH and redox potential are rigorously maintained to maximize selectivity and sorption capacity.

Loaded sorbents are then advanced to the desorption stage, where carefully regulated physicochemical conditions facilitate the release of the captured metals into concentrated eluates. These eluates are further treated through precipitation processes, in which controlled adjustments of pH, reagent dosage, and redox conditions lead to the formation of stable, metal-rich concentrates of high purity.

*Sintering Methodology*

Based on mineralogical and X-ray spectral analyses of the ore, conducted using an electron probe microanalyzer equipped with an energy-dispersive spectrometer, it is evident that all precious components of the ore are encapsulated within a “carbon-silica shell”, which hinders the complete extraction of valuable metals from the ores. Consequently, to disrupt the “carbon-silica shell”, the experiments involving the sintering of

the ore with a mixture of ammonium bisulfate ($NH_4HSO_4$) were conducted. For this purpose, batches with varying mass ratios of ore to ammonium bisulfate were prepared and sintered at the established optimal temperature. The conditions and parameters of the low-temperature roasting process are presented below in Table 4.

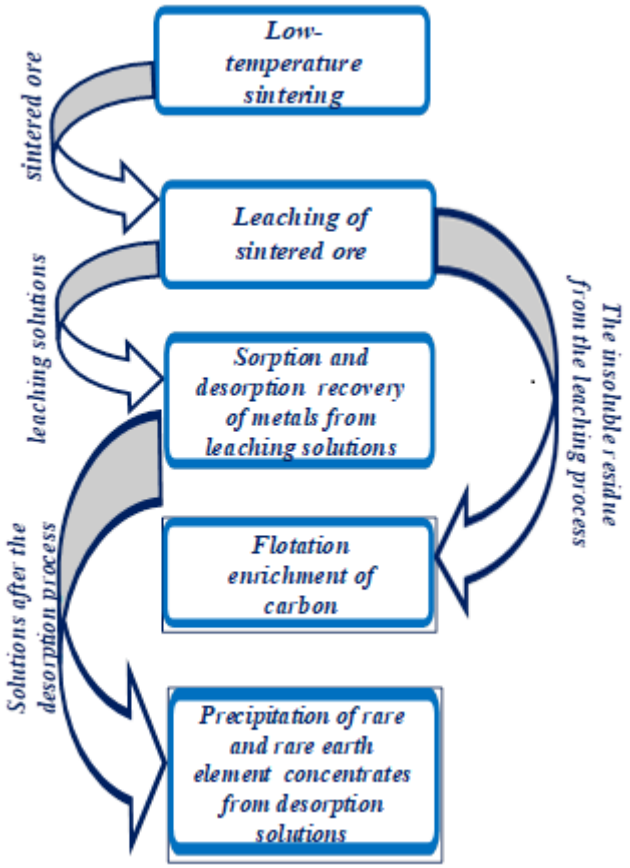



**Figure 2:** Diagram of the research workflow

**Table 4:** Parameters of experimental work on the sintering of black shale ores

| No. | Charge components, g | | Sintering process temperature, °C | Sintering process duration, min |
|---|---|---|---|---|
| | Black shale ore | $NH_4HSO_4$ | | |
| 1 | 100 | 50 | 150-350 | 60 |
| 2 | 100 | 75 | | |
| 3 | 100 | 100 | | |
| 4 | 100 | 125 | | |

During the preparation of the charge, 100 grams of crushed ore were thoroughly mixed with the calculated mass of ammonium bisulfate in a mortar, and the mixture was placed in a preheated furnace. After the specified time had elapsed, the mixture was removed from the furnace, cooled in a desiccator to room temperature, and weighed. Following the determination of the residual mass, the sintered material was directed to leaching.

*Leaching Methodology*

Leaching of black shale ore sinters was employed to extract valuable components such as vanadium, uranium, molybdenum, and rare earth metals into an aqueous solution. Leaching enables more complete extraction of valuable metals from the sinter, thereby increasing the economic efficiency of the process. The process allows for extraction of up to 90% or more of valuable components from the ore and is often

less expensive and less energy-intensive, in comparison compared to high-temperature smelting.

A 50-g sample of sintered product was placed in a sealed glass reactor equipped with a mechanical stirrer and a sampling port for future analyses. The reactor's temperature was maintained under precise control using a thermostat that was accurate to ±1 °C. Before initiating the leaching, the dry sinter material and the vessel were preheated to the desired temperature; subsequently, a preheated separate acid solution was added at the same temperature. Upon the addition of the acid, stirring was initiated immediately, and the elapsed time of the experiment was recorded. Aliquots of pulp (5.0 mL) were withdrawn at defined intervals of 30, 60, 90, 120, 150, and 180 minutes from the sampling port, filtered immediately, and filtrate was diluted to 250 mL for subsequent analysis.

Systematic exploration of the effect of the ratio of solid to liquid phase, between 1:2 and 1:4, and sulfuric acid concentration between 10 and 60 g/L was conducted. Each experimental cycle was duplicated three times to obtain reproducibility, and data were recorded in the form of the average experiments. The glassware of all laboratory equipment was soaked overnight in a 2% sulfuric acid solution, followed by good rinse with high-purity deionized distilled water, which was further used for all stages of dilution procedures throughout the research.

The efficiency of leaching (LE, %) was quantitatively represented by the following Equation [29].

$$LE\ (\%) = \frac{C_A \cdot V}{C_0 \cdot M} \cdot 100 \quad (1)$$

Where, $C_A$ denotes the concentration of metal in the leachate (leach liquor), expressed in grams per liter ($g \cdot L^{-1}$); V represents the volume of leachate, expressed in liters (L); $C_0$ signifies the metal content in sintered mass, expressed as a percentage (%); M indicates the mass of sintered product, expressed in grams (g).

*Flotation Methodology*

The flotation experiments were conducted using a flotation machine equipped with a 1.0 L cell, maintaining an impeller speed of 1,000 rpm during both stages (*i.e.,* conditioning and collection). The experiments were performed at a natural pH range of 7–8. Initially, the sample was mixed with tap water in flotation cell for 3 minutes at a pulp density of 25 % (w/w). Following this, the collector (kerosene) and frother (FLOTOLB) were added. The kerosene dosage was kept constant at 35 g/t, while the FLOTOLB dosage varied between 40 and 70 g/t. The optimal kerosene dosage of 35 g/t was determined through bench-scale flotation tests, which showed that increasing the kerosene dosage from 10 to 35 g/t improved C-matter recovery from 40% to 82 % (with a feed particle size of 85 % passing 0.074 mm). Subsequent tests on the influence of FLOTOLB were conducted using 35 g/t of kerosene. Conditioning times for kerosene and FLOTOLB were set at 1 minute each, with kerosene added first, followed by FLOTOLB. To ensure accuracy, all tests were repeated, and final recoveries demonstrated negligible differences of less than 3 %. The flotation tailings and carbon concentrate were dried at 60 °C for 24 hours and weighed to measure the product yield. The carbon content was analyzed using an ELTRA CS-2000 analyzer. The flotation efficiency (FE) was calculated using following equation [30]:

$$FE = \frac{\gamma \cdot \beta}{\alpha} \cdot 100 \quad (2)$$

Where, γ denotes the mass of carbon concentrate, expressed as m; β represents the carbon grade

within concentrate, quantified as percentage (%); α signifies the carbon content present in sintered material, also presented as a percentage (%).

*Sorption Concentration*

The sorption extraction of uranium, molybdenum, vanadium, and rare earth metal (REM) ions from solutions acquired after leaching the sintered mass of black shale ore constituted subsequent phase of the current investigation. The primary objective of the present investigation was to achieve selective extraction and concentration of individual metals from multicomponent solutions. Selectivity became affordable by meticulously controlling the redox potential (Eh) and acidity (pH) of the solutions. Specific Eh and pH values were required for each metal to ensure optimal sorption. By regulating such parameters, effective separation of metal ions was achieved, thereby minimizing losses. It is noteworthy that results of the desorption studies of rare and rare earth metals from saturated ion exchangers were briefly summarized, highlighting the most effective desorbing solutions, while omitting results of other investigated solutions. Comprehensive data on all studied desorbing solutions, their performance indicators, and the kinetic patterns of the processes will be detailed in a subsequent publication.

It should also be noted that this article does not present the results of the sorption selective extraction of uranium, as these findings were previously published by our research team [21]. In the previously published article, the methodology and rationale for employing the anion-exchange method for uranium extraction are discussed, including the sorption characteristics of the four investigated weakly basic and strongly basic anion exchangers, the effect of the pH environment, and the duration of the process. The main outcomes indicated that strongly basic anion-exchange sorbents offer the best performance for uranium extraction, achieving up to 90% efficiency at pH 2.2 and a duration time of 12 hours. To elucidate the kinetics of sorption, pseudo-first-order, pseudo-second-order, and intraparticle diffusion models were utilized. The outcomes of mathematical modeling suggested that uranium sorption can be well described by the pseudo-second-order kinetic model. Equilibria were characterized by exploitation of Langmuir, Freundlich, and Dubinin–Radushkevich equations.

*Methodology for the Sorption Concentration and Desorption of Molybdenum*

For the investigation of the selective sorption extraction of molybdenum, solutions obtained after uranium sorption at pH 2.2 were utilized. It is well known that molybdenum can exist in either anionic form (at pH above 2.0 - 2.2) or cationic form (at pH below 2.0), depending on the pH of the solution [31,32]. Consequently, molybdenum ions in cationic form are present only in strongly acidic solutions. If cation sorption is conducted under these conditions, other impurity metal cations, such as iron and aluminum, whose concentrations are several times higher than those of molybdenum, may also be sorbed. Based on this literature data, an anion-exchange sorption method was employed at pH 2.5 in previous studies, which allows molybdenum to be converted into an anionic form and ensures the selectivity of molybdenum extraction. To adjust the solution to pH 2.5, ammonia was added while stirring, with a consumption of 1.2 mL per 100 mL of solution.

Experiments on molybdenum sorption were conducted in 150 mL conical flasks in a static mode using overhead stirring devices at room temperature. The concentrations of rare and rare earth metals in the solution were, in g/dm$^3$: Mo-0.113; V-1.96; REM-0.23; total Fe-8.8; Al-0.53. For the sorption experiments, portions of sorbent (1.0 g) were mixed with solutions (100 mL), and the process of sorbent saturation with molybdenum was continued until equilibrium between the sorbent and the solution was reached. The analysis of molybdenum content in the sorption solution was conducted at 360, 540, 720, 900, and 1,440 minutes (every 3 hours) after the start of the process. The objective of current research was to determine the time required to

achieve maximum saturation of the investigated anion exchangers Ambersep 920 and Purolite A100.

$$SE = \frac{C_i - C_f}{C_i} \cdot 100 \quad (3)$$

Where, $C_i$ and $C_f$ are initial and final concentrations of metals in solutions, respectively.

*Methodology for the Sorption Concentration and Desorption of Vanadium*

To assess the selective sorption extraction of vanadium, the solutions obtained after molybdenum sorption at pH 2.5, containing rare and rare earth metals (in g/dm$^3$: V-1.96; REM-0.23; total Fe-8.8; Al-0.53), were utilized. Under these conditions, *i.e.,* at pH 2.5, vanadium existed in cationic form. To successfully implement the sorption extraction of vanadium, the pH of the solution was adjusted to 1.6-1.7 using sulfuric acid, followed by the addition of a 33% hydrogen peroxide solution to oxidize vanadium to its pentavalent form and convert it to an anionic form, with a consumption of 1.3 ml per 100 ml of solution. The oxidation process of vanadium to the pentavalent state was conducted at 60 °C. Using hydrogen peroxide, the Eh of the solution was adjusted to 800-850 mV, ensuring that all vanadium was in the anionic pentavalent form. Subsequently, the sorption extraction process was carried out in a static mode, using a methodology similar to that applied for the sorption of molybdenum anions. The analysis of vanadium content in the solution was conducted at 120, 240, 360, 480, 600, and 720 minutes after the initiation of the process. The objective of the study was to determine the time required to achieve maximum saturation of the investigated anion exchangers Ambersep 920 and Purolite A100 with vanadium. Each vanadium sorption experiment was repeated three times, and the results were averaged. The degree of vanadium extraction was calculated using Equation (3).

Experiments on the desorption of vanadium from anion exchangers were conducted under static mode conditions similar to the molybdenum desorption process. Sodium hydroxide solutions with concentrations ranging from 3.0 to 12.0% were used as desorbing solutions. The process was conducted under static conditions with a ratio of anion exchangers to desorbing solution of 1:10. After adding the desorbing solution to the flask containing the saturated anion exchangers, stirring commenced and the experiment time was recorded. The analysis of desorbed vanadium content from the anion exchangers was conducted at 60, 120, 180, 240, and 360 minutes after the initiation of the process. The objective was to determine the minimum duration required to achieve maximum desorption of vanadium ions from the anion exchangers.

*Methodology for the Sorption Concentration and Desorption of REM*

To investigate the selective sorption extraction of rare earth metals (REM), solutions obtained after vanadium sorption at pH 1.6-1.7, containing REM at 0.23 g/dm$^3$, were used. To successfully implement the sorption extraction of REM, the pH of solutions was adjusted to 2.0 using ammonia solution, with a consumption of 0.8 mL per 100 mL of solution. Subsequently, the sorption extraction process was conducted in a static mode, using a methodology similar to that applied for the sorption of molybdenum and vanadium anions, with stirring by a shaker. The analysis of REM content in the solution was conducted at 30, 60, 90, 120, and 150 minutes after the start of the process. The objective of the current investigation was to determine the time required to achieve the maximum saturation of the investigated cation exchangers KU-2-8H with REM. Similar to the studies on molybdenum and vanadium extraction, each REM sorption experiments was repeated three times, and averaged results were reported. The degree of REM extraction was calculated using Equation 3.

Experiments on the desorption of REM from cation exchangers were conducted under static conditions similar to the molybdenum and vanadium desorption processes. A sulfuric acid solution with a concentration of 100 g/dm$^3$ was used as the desorbing solution. The process was conducted under static conditions with a ratio of cation exchangers to desorbing solution of 1:10. After adding the desorbing solution to the flask containing the saturated cation exchangers, stirring commenced and the experiment time was recorded. The analysis of desorbed REM content in the solution was conducted at 30, 60, 90, 120, and 150 minutes after the start of the process. The objective of the process was to determine minimal duration required to achieve maximum desorption of REM ions from the cation exchangers.

*Methodologies for the Precipitations*

*Methodology for the Precipitation of Calcium Molybdate (Molybdenum Concentrate)*

Experiments on the precipitation of calcium molybdate ($CaMoO_4$) were conducted in a thermostatically controlled environment equipped with a mechanical stirring apparatus. The aqueous-phase molybdenum was converted into calcium molybdate at a pH of 8.9 to 9.0 by incrementally adding calcium chloride ($CaCl_2$) until a molar ratio of ($Ca^{2+}$):(Mo) = 3:1. This process was carried out under continuous stirring and maintained at 85 ± 2 °C. After a specified mixing duration, ranging from 30 to 240 minutes, to determine the optimal time for $CaMoO_4$ formation, the reactor containing the combined solutions of molybdenum desorbate and $CaCl_2$ was transferred to another reactor. In this secondary vessel, the temperature was regulated at 25 ± 2 °C, and mixing was continued until the $CaMoO_4$ precipitation was complete. Following the precipitation, the $CaMoO_4$ precipitate was separated through filtration, and the dried product at 95 ºC product was subsequently analyzed.

*Methodology for the Precipitation of Ammonium Metavanadate (Molybdenum Concentrate)*

The desorbate obtained from the vanadium desorption experiments (methodology described in Section 4.4.2) was utilized for the crystallization of ammonium metavanadate. The precipitation experiments were conducted in thermostated glass reactors equipped with stirring devices. The desorbate solution was placed in the reactor, and an ammonium sulfate solution with a concentration of 50 g/L was added dropwise until the required molar ratio of ammonium sulfate to vanadium of 3:1 was achieved. The crystallization process of ammonium metavanadate was carried out at a temperature of 15 ± 2°C with constant stirring. Crystallization continued with continuous stirring and periodic analysis of vanadium content in the solution every 30 minutes until the decrease in vanadium concentration ceased. Upon completion of the precipitation process, ammonium metavanadate was separated by filtering, washed with water on the filter, and dried at 95 °C to a constant weight.

*Methodology for the Precipitation of REM Concentrate*

The desorbate obtained from the rare earth metals (REM) desorption experiments, as described in Section 4.4.3, was utilized for the precipitation of REM concentrates. The experiments were conducted in thermostated glass reactors equipped with stirring devices. The REM desorbate solution was placed in the reactor, and sodium carbonate was added as required for the precipitation of the target concentrates. The precipitation process was carried out at 15 ± 2 °C with constant stirring. Precipitation continued with continuous stirring and periodic analysis of the rare earth metal content in the solution every 30 minutes until the decrease in their concentration ceased. Upon completion of the precipitation process, the precipitate was separated by filtration, washed with distilled water on the filter, and dried at 95 °C in a muffle furnace to a constant weight.

## Results and Discussion

*Low-Temperature Sintering of Black Shale ore*

*Effect of ore to Ammonium Hydrosulfate Ratio*

The physicochemical analyses of black shale ore demonstrate that vanadium is predominantly present as V(III), with V(V) being virtually absent. This reality significantly complicates the extraction process via direct leaching, as V(III) and its compounds are insoluble in water or acid solutions, unlike V(IV) and V(V). A thorough review of the literature [33-35] identifies two critical factors for enhancing vanadium extraction efficiency: the disintegration of the ore's structure to liberate vanadium and the oxidation of V(III) to V(IV) or V(V). Various high-temperature oxidation techniques, such as roasting and thermal activation above 800 °C, have been employed by researchers [36,37], although these methods are energy-intensive due to the substantial energy required to achieve high temperatures. Direct acid leaching of raw black shale typically requires harsh conditions, such as the use of $H_2SO_4$–HF mixtures at temperatures ≥95 °C and durations ≥6 hours. Under these conditions, vanadium dissolution is limited by mass transfer constraints imposed by the stable silicate matrix [38]. Pretreatment via low-temperature roasting significantly reduces the energy barrier and transforms vanadium into coordination-flexible complexes ($VO^{2+}$/$VO_2^+$) in a sulfate medium, thereby enhancing leaching kinetics. Comparable studies on thermally activated black shales or shale concentrates report vanadium recoveries of 70–86% within 3–6 hours at 80–95 °C [39]. The present study investigates sintering of black shale ores at temperatures below 350°C, exploiting ammonium hydrosulfate to evaluate the decomposition of ore. Such a process facilitates breakdown of the "carbon-silica shell" and, therefore, alters the ore structure and improves access for leaching reagents. Some experiments were conducted to assess the impact of ammonium hydrosulfate consumption on carbon removal, with different ratios ranging from 0.5:1 to 1.25:1, at 350°C. The optimal ore-to-hydrosulfate ratio was determined to be 1:1, leading to remarkable ore mass exposure and effective destruction of the "carbon-silica shell". The sintered product appeared as a fused mass (Figure 3), revealing the success of the adopted procedure in enhancing vanadium extraction from black shale ore, while offering a lower energy consumption alternative to traditional high-temperature processes.



**Figure 3:** The resulting sinter

The essence of the process is that when a mixture of ore and ammonium hydrosulfate is heated, chemical reactions occur, leading to the removal of crystalline bound water. Additionally, a molten mass is formed and rare and rare-earth metals are converted into water-soluble sulfate salts.

*Effect of Temperature On The Sintering Process*

Experiments on the temperature effect on the carbon removal and structural destruction of the "carbon-silica shell" were performed in a muffle furnace within the temperature range 150–350 °C with an ammonium hydrosulfate to ore ratio of 1:1. The results, as presented in Figure 4, show that increased temperatures manage to guarantee effective removal of carbon from the "carbon-silica shell". This process significantly enhances the permeability of the shell and hence the access of leaching reagents to rare and rare earth metals and promotes more effective extraction.

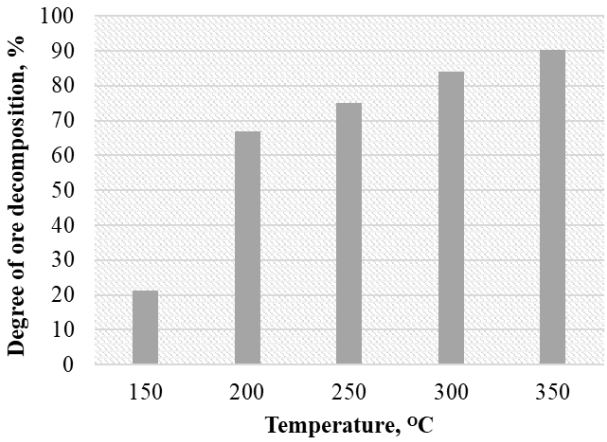



**Figure 4:** Degree of ore decomposition depending on the temperature of the sintering process

The data reveal that at 150 °C, the ore undergoes 20–21% decomposition (approximately), accompanied by partial disintegration of the carbon-silica shell. In comparison, at 350 °C, the degree of ore decomposition significantly rises to about 90%, a process driven by the elimination of crystallized bound waters and the extensive breakdown of the carbon-silica shell. Such observations are substantiated by thermogravimetric analysis (TGA) (see Figure 5, Table 2), which distinctly delineates the chemical compositional alterations occurring during heating and offers detailed insights into transformations at the molecular level.

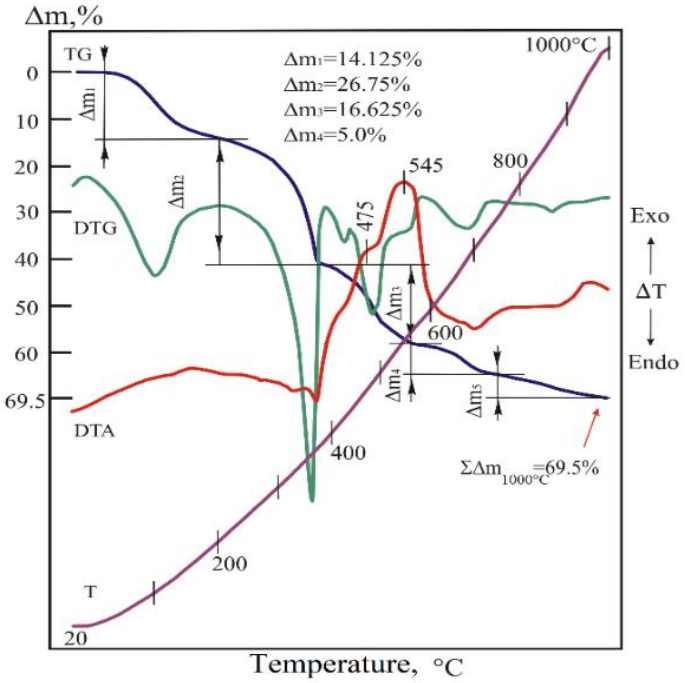



**Figure 5:** Derivatogram of low-temperature ore decomposition

During the sintering of the ore at temperatures between 100 °C and 350 °C (zone $m_1$), both crystallization and chemically bound water are eliminated through dehydration and decarbonization processes (Table 5). This results in a mass loss of 14.125% for the sample.

**Table 5:** Thermogravimetric indicators of the sintering process within the range of 20-1,000°C

| Stages of weight loss during heating | Temperature spans of weight loss (decomposition stages), °C | Estimated emissions at corresponding decomposition stages | Amount of weight loss, % |
|---|---|---|---|
| $\Delta m_1$ | 20-385 | $H_2O$ and $CO_2$ | 14.125 |
| $\Delta m_2$ | 385-570 | CO, H, and NO | 26.75 |
| $\Delta m_3$ | 570-650 | CO and H | 16.625 |
| $\Delta m_4$ | 650-735 | $CO_2$, H, and N | 5.00 |
| $\Delta m_5$ | 735-1,000 | $CO_2$, H, N, and $SO_2$ | 3.25 |
| $\sum \Delta m_{1000°C}$ | 20-1,000 | $H_2O$, C, H, N, $NO_2$, $CO_2$, and $SO_2$ | 69.5 |

To understand the behavior of ore components during high-temperature treatments, the mechanisms of reactions occurring upon further heating of samples up to 1,000 °C were considered. Dynamic heating of the original ore within the range of 20-1,000 °C revealed a series of endothermic and exothermic reactions associated with the partial decomposition of zeolites and carbonates present in the black shale ore. As seen from results of thermogravimetric analysis, further heating of the ore in the temperature range of 385-570 °C leads to decomposition of ore components with the release of CO, $H_2$, and $N_2$ gases (region $\Delta_{m2}$), which apparently correspond to easily decomposable carbonate minerals and micas, such as vanadium-containing siliceous roscoelites and phengites. The endothermic effect observed at 545 °C is related to the enantiotropic polymorphic transformation of quartz, which further confirms the processes involving changes in the structure of silicon-containing components. Further heating of the ore in the temperature ranges of 570-650 °C and 650-735 °C results in the decomposition of hard-to-decompose minerals such as montroseite, duttonite, and other spinel-type oxides, where vanadium is present in forms of $V^{2+}$ and $V^{3+}$. The data on the decomposition of these minerals at corresponding temperatures are confirmed by the studies of Chen [40]. Heating of the sample to 1,000 °C is accompanied by the decomposition of aluminosilicate minerals such as muscovite and kaolinite, sulfides such as sulvanite and patronite, and residual carbon-containing minerals. The difficulty in decomposing aluminosilicates such as muscovite and kaolinite is also noted in the studies of Zhou [41], who suggested that their decomposition occurs at temperatures above 900 °C. The authors claim that leaching of sinters obtained after roasting at such temperatures can achieve higher vanadium extraction efficiency. However, at temperatures above 950 °C, sintering of the material occurs, forming a dense layered structure that hinders vanadium leaching. Additionally, at such temperatures, the valuable carbon component of the shale is senselessly burned off. Therefore, to avoid the aforementioned negative effects such as high energy consumption at elevated temperatures, loss of valuable carbon, and the formation of obstructive dense structures, we conducted sintering processes at 350 °C with ammonium hydrosulfate. During this process, transformation of silica from amorphous form to a stable crystalline with an ordered arrangement was observed, which is confirmed by the results of FTIR analysis (Figure 6).

The FTIR analysis reveals the existence of a prominent band in the sinter samples, with a maximum at wavenumbers 3,128–3,027 $cm^{-1}$, indicative of ammonium hydrosulfate and α-$SiO_2$ quartz. The α-$SiO_2$ quartz displays characteristic bands at 798, 779, 694, 512, and 459 $cm^{-1}$. Additionally, intense bands with maxima at wavenumbers 1120, 675, and 599 $cm^{-1}$,

assignable to gypsum, and muscovite $KAl_2[(OH,F)_2$, with bands at 1,032 and 434 $cm^{-1}$, are observed [42]. Such findings herald the complex mineralogical composition of sinter samples and provide information about chemical interactions occurring during the sintering process.

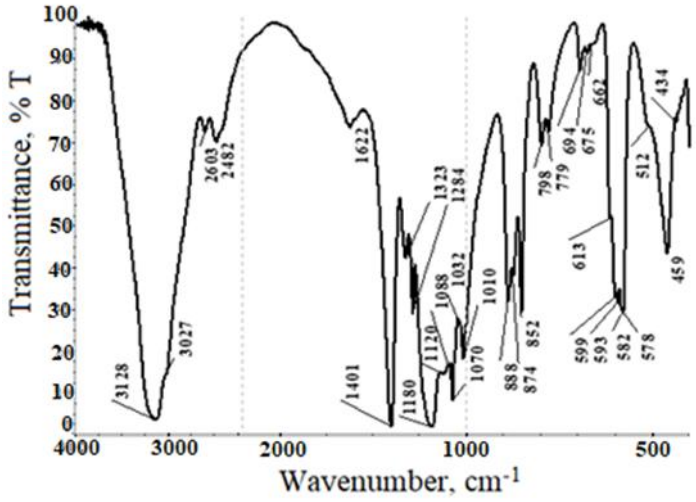



**Figure 6:** FTIR analysis of the resulted sinter

*Leaching of Sinters*

Low-temperature sintering effectively facilitated the near-complete removal of the "carbon-silica shell" and transformed rare and rare earth metals into a readily soluble form. Subsequently, the leaching of the sintered product was conducted under various conditions, as detailed in the methodology outlined in Section 4.2.

*Effect of sulfuric Acid Concentration*

Table 6 shows recoveries of vanadium, uranium, molybdenum, and rare earth metals achieved by varying the sulfuric acid content between 10 and 60 g/L. The evidence clearly shows that the increase in sulfuric acid content to 40 g/L significantly enhances the leaching efficiency of uranium, vanadium, molybdenum, and rare earth metals. Increases in acid concentration beyond 40 g/L do not yield significant enhancements. This indicates that the system has reached a point of saturation, where parameters such as insufficient chemical reaction time, saturation, or availability of reactive sites become limiting.

**Table 6:** Results of leaching the sintering process product at different sulfuric acid concentrations

| Concentration of sulfuric acid at the beginning of leaching, g/L | Concentration, g/L<br>Leaching efficiency, % | | | | | | | |
|---|---|---|---|---|---|---|---|---|
| | V | | U | | Mo | | REM | |
| | g/L | % | g/L | % | g/L | % | g/L | % |
| 10 | 0.81 | 30.2 | 0.044 | 57.5 | 0.058 | 41.7 | 0.079 | 26.4 |
| 20 | 1.27 | 47.4 | 0.056 | 72.1 | 0.081 | 58.4 | 0.123 | 41.2 |
| 30 | 1.77 | 66.0 | 0.064 | 83.7 | 0.100 | 71.6 | 0.172 | 57.8 |
| 40 | 2.19 | 81.7 | 0.072 | 93.3 | 0.115 | 82.2 | 0.234 | 78.3 |
| 60 | 2.21 | 82.4 | 0.073 | 93.6 | 0.116 | 83.0 | 0.235 | 78.5 |

Such results indicate that while an initial augmentation in sulfuric acid concentration enhances the leaching process, further additions result in diminishing returns due to inherent

constraints. The optimal leaching conditions were achieved at a sulfuric acid concentration of 40 g/L for 120 minutes, resulting in extraction efficiencies of 81.7% for vanadium, 93.3% for uranium, 82.2% for molybdenum, and 78.3% for rare earth metals (REM). Subsequent experiments confirmed that increasing the level of sulfuric acid beyond 40 g/L had a slight effect on extracting these valuable metals, implying that this is a point at which efficiency and resource utilization are optimized.

*The effect of Solid - Liquid Ratio*

To elucidate the reasons for incomplete extraction of target metals, which may include factors such as solution saturation, insufficient leaching time, or reduced availability of reactive sites, studies were conducted to evaluate the impact of various parameters, including process duration and the solid-to-liquid ratio. The ratio of liquid to solid phase during leaching is a critical determinant of leaching efficiency and effectiveness [43]. Therefore, optimizing this ratio is essential for maximizing extraction efficacy. Alteration in the solid-to-liquid ration from 1:2 to 1:4, as shown in Table 7, had minimal impact on the extraction of vanadium, uranium, molybdenum, and rare earth metals. A minimal ratio of 1:2 was selected for further investigations, as a 1:1 ratio resulted in the fabrication of a viscous mass that hindered mixing and prevented effective extraction of valuable metals. Mixing during leaching is crucial as it facilitates free diffusion of reactive substances into the leaching solution. The leaching process comprises five diffusion stages [44].

1) Diffusion of leaching reagent to the surface of the solid phase (material obtained after sintering);
2) Diffusion of the leaching reagent through the solid product layer via interconnected pores and cracks to the valuable metals;
3) Chemical reaction forming new products (*e.g.,* vanadium, uranium, molybdenum, and rare earth metal sulfates);
4) Diffusion of the new products from the reaction zone to the surface of the solid material through pores and cracks; and
5) Diffusion of the products from the surface of the solid material into the solution volume.

The entire leaching process and the extraction of valuable components are directly dependent on diffusion within the leaching medium. Therefore, ensuring free diffusion in the reaction environment is crucial for the successful progression of all anticipated processes.

**Table 7:** The effects of solid-liquid ratio

| Solid-to-Liquid ratio | Concentration, g/L<br>Leaching efficiency, % | | | | | | | |
|---|---|---|---|---|---|---|---|---|
| | V | | U | | Mo | | REM | |
| | g/L | % | g/L | % | g/L | % | g/L | % |
| 1:2 | 1.82 | 67.8 | 0.057 | 74.6 | 0.101 | 72.2 | 0.189 | 63,3 |
| 1:3 | 2.19 | 81.7 | 0.072 | 93.3 | 0.115 | 82.2 | 0.234 | 78.3 |
| 1:4 | 2.19 | 81.7 | 0.073 | 94.8 | 0.118 | 84.4 | 0.236 | 79.2 |

The present findings are consistent with the literature in the field. Of special note, Binnemans *et al.* have demonstrated that lowering the solid-to-liquid ratio below 1:2 leads to lower metal extraction, primarily due to solution saturation effects [45]. On the other hand, Kenzhaliyev *et al.* observed that increasing the solid-to-liquid ratio above 1:3 resulted in reduced metal content in the solution, which they attributed to over-dilution and difficulty in treating high volumes of solution in subsequent processes [46]. The research collectively suggests that maintaining at least 1:3 solid-to-liquid ratio is economically beneficial, as going below this threshold not only reduces efficiency of extraction, but also raises sorption costs along with the extraction of valuable constituents. Thus, 1:3 solid-to-liquid

phase ratio is the optimal compromise between efficiency and economy.

*The effect of Leaching Time*

Experiments were conducted to establish the influence of leaching time on vanadium, uranium, molybdenum, and rare earth metal extraction efficiency for varying leaching times of 30 to 180 minutes. Leaching was done at 80 °C at a solid-to-liquid ratio of 1:3 with an acid concentration of 40 g/L sulfuric acid. Figure 7 shows results obtained from experiments.

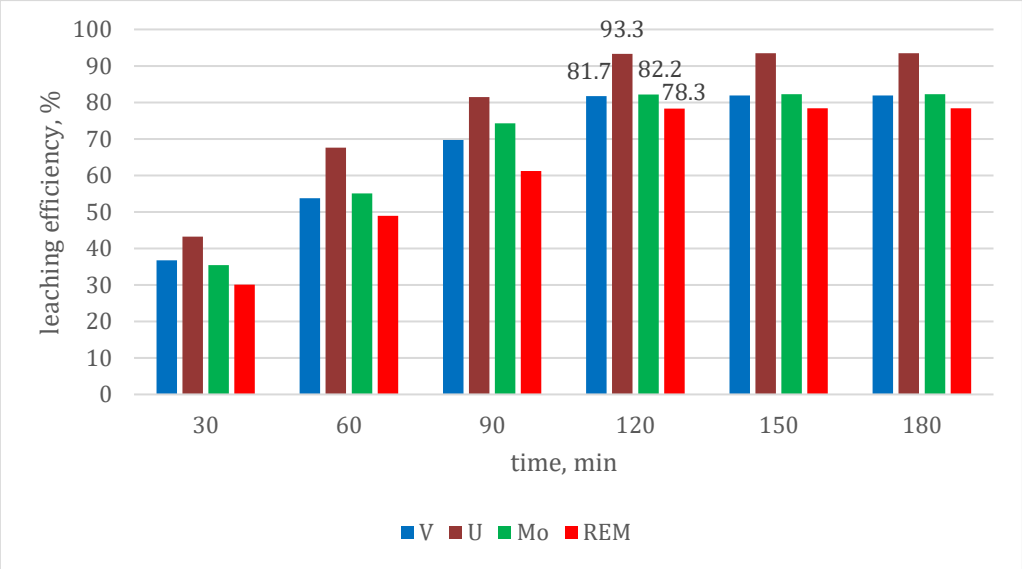



**Figure 7:** Leaching efficiency of V, U, Mo and REM versus reaction time at 80 °C, 40 g/L $H_2SO_4$ and a liquid/solid ratio of 1:3 mL/g

The data presented in the figure indicate that the extraction efficiency of valuable components into the solution increases with the duration of the leaching process. Specifically, vanadium extraction rises from 36.7% at 30 minutes to 81.9% at 180 minutes; uranium extraction increases from 43.2% to 93.5%; molybdenum extraction improves from 35.4% to 82.3%; and rare earth metals (REM) extraction enhances from 30.1% to 78.4%. A detailed analysis reveals that significant extraction occurs up to 120 minutes, and only marginal augmentations (up to 2.0%) observed at 150 and 180 minutes. Such a phenomenon can be attributed to two primary factors:

Firstly, it is likely that all easily decomposing compounds of uranium, molybdenum, vanadium, and REMs formed during sintering with ammonium hydrosulfate have already been leached out. Secondly, this can be attributed to the law of mass action, which states that the speed of a chemical reaction is directly proportional to the concentration of the reactants. At the first stage, the high concentration of acid promotes intensive extraction. As the acid concentration reduces, the reaction rate becomes slower, thus accounting for the progressive increase in extraction efficiency beyond 120 minutes.

Based on these findings, the optimum time for the leaching process was determined to be 120 minutes, which maximizing the efficiency and resource utilization.

*The Effect of Leaching Temperature*

Temperature significantly affects leaching, governing both kinetics and overall efficiency of metal extraction. Higher temperatures enhance molecular movement, which accelerates reaction rates and facilitates more effective dissolution of targeted components. Conversely, lower temperatures reduce molecular activity, resulting in lower leaching kinetics and extended processing periods to achieve equivalent

extraction levels. Hence, careful assessment of the effects of temperature is imperative for enhancing leaching efficiency against production costs. In addition to temperature, fine control of other variables-such as reagent concentration and S:L ratio-is also essential for maximum extraction yields with minimal loss through side reactions or leaching incompleteness. Optimal control of these variables ensures efficient recovery of metal values from ore matrices.

In the present work, the leaching properties of products from sintering black shale ores with ammonium hydrosulfate were studied systematically. The experimental design tested the influence of temperature and duration of extraction on the extraction rates of the main valuable constituents. Leaching tests were conducted at 20 °C, 40 °C, 60 °C, and 80 °C with an initial concentration of sulfuric acid of 40 g/L, a fixed contact time of 120 minutes, and a solid-to-liquid ratio of 1:3. The corresponding leaching efficiencies provided in Figure 8 include crucial information on the interaction between heat conditions and extraction behavior and thus dictate the selection of optimum process parameters for actual application.

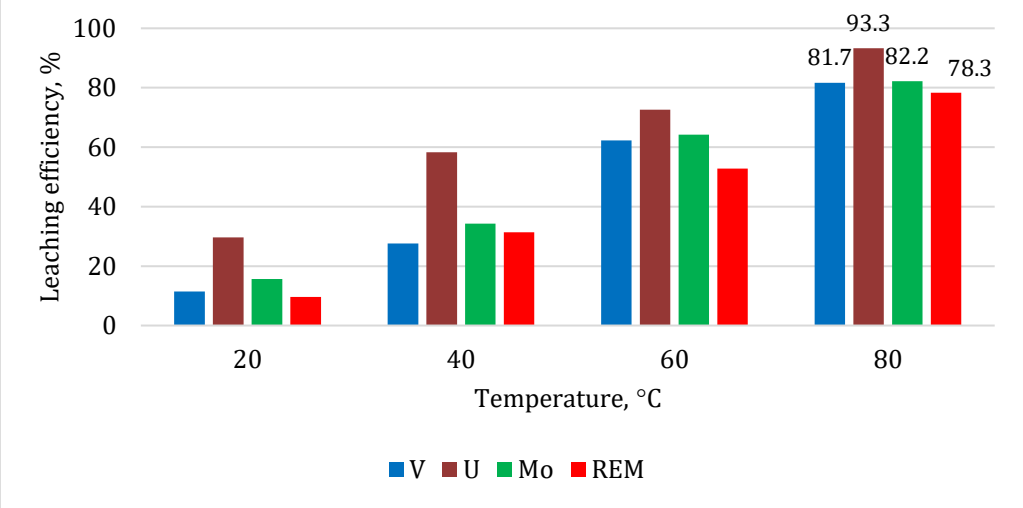



**Figure 8:** Leaching efficiency of V, U, Mo and REM versus reaction Temperature at 120 min, 40 g/L $H_2SO_4$ and a liquid/solid ratio of 1:3 mL/g

Figure 8 clearly indicates that increasing the leaching temperature significantly enhances the extraction efficiency of vanadium, uranium, molybdenum, and REM. Specifically, the leaching efficiency of REMs increases from 9% at 20°C to 78.3% at 80°C. Similarly, the extraction efficiencies of vanadium, uranium, and molybdenum are enhanced from 11.5% to 81.7%, 29.6% to 93.3%, and 15.6% to 82.2%, respectively, when the temperature is increased from 20 °C to 80 °C. This is accounted for by Van't Hoff's law, demonstrating that the rate of chemical reactions is increased by temperature. Molecules possess more kinetic energy at high temperatures and, therefore, collide more frequently and, in so doing, the reaction rate is boosted. However, above 80 °C, vigorous evaporation of the leaching solution can negatively affect the process through pulp thickening and reduced diffusion transfer in the leaching system. The same results on improving vanadium extraction efficiency with higher leaching temperature were obtained by Li *et al.* [5], where they observed that vanadium extraction rose from 43% at 45 °C to 85% at 95 °C. Interestingly, their duration of the leaching process was 6 hours, while our research managed to accomplish the same in only 2 hours.

The experimental study by other researchers [47], on oxidative autoclave leaching extraction of vanadium and molybdenum from black shales, further confirms these results. Leaching was performed in two stages: in stage 1, vanadium was extracted with a yield of 86.81% under conditions of 35 wt.% $H_2SO_4$, 4 wt.% $CaF_2$, a liquid to solid ratio 1.2:1 (L/kg) at 95 °C for 8

hours. In the second step, leaching of molybdenum was accomplished with 91.10% recovery under 25 wt.% $H_2SO_4$, 8 wt.% $NaClO_3$, a 1.5:1 (L/kg) liquid-solid ratio, at 45 °C for 7 hours. The study evidently demonstrates the feasibility of lode/residual autoclave oxidative leaching to recover precious metals from black shales. The elevated efficiencies of molybdenum and vanadium leaching under certain conditions highlight the commercial feasibility of the process. The use of different reagents and conditions in each step allowed for selective extraction of each metal, reflecting the versatility of the process alongside its precision. It should, however, be noted that autoclave leaching is inherently a resource-intensive and complex process, particularly when scaled up for large-volume production. The high pressures and temperatures of autoclave units pose formidable challenges regarding process control and safety. In hydrometallurgical plants, autoclaves have been likened to "bombs" due to the dangers posed by their operation under pressure.

*Analysis of Leaching Residues and Flotation Enrichment*

To achieve a more effective utilization of mineral resources, an extensive amount of research has been directed toward flotation extraction of carbon from leaching residues. Carbonaceous materials have been in high demand due to their high strength, rigidity, and wear resistance properties, making them indispensable for structural applications and tool manufacturing. Carbon steel is widely used in mechanical engineering for fabricating machine parts, tools, and equipment [48,49]. The energy and aerospace industries highly value carbonaceous materials for their impressive combination of strength and lightweight properties, making them ideal for constructing aircraft components. Additionally, there is a growing trend toward using carbon as the primary material for constructing the bodies of high-speed automobiles [50]. Extracting carbonaceous materials from industrial by-products obtained through existing technologies expands the product range and contributes to the further development of ore raw materials.

The insoluble leach residue, which was yielded under ideal conditions of operation (temperature = 80 °C, time = 2 hours, solid : liquid ratio = 1:2, acid concentration = 40 g/L sulfuric acid), constituted 81.6% of the original mass that was subjected to leaching. This leach residue was then analyzed chemically and by FTIR spectrophotometry, the data of which are presented in Table 8 and Figure 8. Based on Table 9, it is clear that the leaching residue primarily contains silicon dioxide ($SiO_2$ ~ 79.9%) and carbon, with the carbon content increasing from 14.72% to 17.89%.

**Table 8:** Chemical composition of the insoluble residue from the leaching process (cake)

| Contents, % | | | | | | | |
|---|---|---|---|---|---|---|---|
| **V** | **U** | **Mo** | **REM** | **Fe** | **Al** | **Si** | **C** |
| 0.16 | 0.001 | 0.009 | 0.02 | 0.21 | 0.05 | 37.3 | 17.89 |

This carbon concentration is quite satisfactory, as materials with similar carbon content are used in the production of carbon concentrates.

The FTIR analysis of the leaching residue (Figure 9) exhibits the presence of an intense band with a maximum at wavenumbers 3427–3126 $cm^{-1}$, indicative of carbon and α-$SiO_2$ quartz. The α-$SiO_2$ quartz exhibits characteristic bands at 1167, 1089, 797, 778, 694, 510, and 462 $cm^{-1}$. Additionally, an intense band with a maximum at 834 $cm^{-1}$, corresponding to vanadium-containing hard-to-extract spinels, and the $[SO_4]^{2-}$ group at 600, 592, and 582 $cm^{-1}$, is observed.

Following the determination of the chemical composition and properties of the leaching residue, studies on the flotation enrichment of carbon were conducted as per the methodology described in Section 4.3. According to this methodology, kerosene consumption during flotation enrichment was 35 g/t, and the

consumption of the flotation reagent FlotolB ranged from 40 g/t to 70 g/t (Table 9, Figure 10).

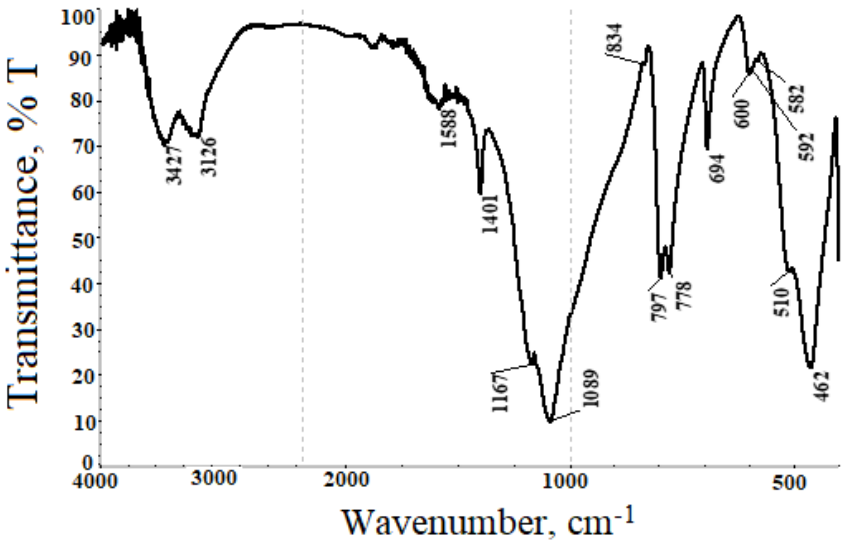



**Figure 9:** FTIR analysis of the insoluble residue from the leaching process



**Figure 10:** The process of flotation enrichment

Table 9 indicates that increasing the dosage of the flotation reagent enhances the carbon content in the concentrate, while the overall yield of the concentrate from the total mass declines. Such an adjustment results in a more carbon-rich product. Notably, when flotation enrichment is performed with a reagent dosage of 40 g per ton of ore, there is no significant carbon enrichment; the carbon is approximately evenly distributed between the concentrate and the tailings. However, increasing the reagent dosage to 70 g per ton leads to a noticeable concentration of carbon in the froth product (concentrate).

**Table 9:** Results of flotation enrichment experiments

| FlotolB consumption | Enrichment products | Yield of product from total mass, % | Carbon content in the products, % | Distribution of carbon across enrichment products, % |
|---|---|---|---|---|
| 40 g/t | Concentrate | 57.3 | 18.85 | 60.6 |
| | Tailings | 35.7 | 19.85 | 39.4 |
| 50 g/t | Concentrate | 52.17 | 27.5 | 79.7 |
| | Tailings | 47.83 | 7.64 | 20.3 |
| 60 g/t | Concentrate | 43.7 | 35.9 | 87.1 |
| | Tailings | 56.3 | 4.10 | 12.9 |
| 70 g/t | Concentrate | 41.4 | 38.5 | 88.9 |
| | Tailings | 58.6 | 3.31 | 10.8 |

A careful scrutiny of the experimental data indicates that an increase in the reagent dosage from 70 to 80 grams per ton results in a minor rise in the carbon recovery in the concentrate by 1.8%. On the contrary, an increase in the dosage of the reagent from 60 to 70 grams per ton results in a very significant rise in the carbon recovery of more than 7.4%. This means that the optimal reagent dosage for the maximum carbon recovery is 60 grams per ton. The findings have been corroborated by previous studies on flotation optimization. For instance, Li *et al.* [51] optimized the collecting agents employed in spent pot lining flotation and observed that raising the dosages did improve recovery, but the increment started to plateau after some point. Researchers achieved a 73% carbonaceous matter recovery and combined cleaner concentrate grade of 4%, while Lee *et al.* [52] optimized the collector agents to achieve carbon grades and recovery of concentrate over 80% and 95%, respectively.

*Processing of Leaching Solutions*

The leaching operation yields two distinct products: (1) an undissolved solid residue with a principal composition of silicon oxide and carbon, and (2) an ion-bearing solution of vanadium, molybdenum, uranium, and REMs. Based on the developed technology, this ion-bearing solution undergoes further processing through selective extraction methods using sorption processes. In the current study, the following step of research aimed to determine the optimal parameters for effective and selective recovery of these valuable metals from the leachate using sorption refining procedures.

*Molybdenum Sorption*

The molybdenum sorption study, conducted according the experiment in experimental section, was to determine the effect of process time on molybdenum anion sorption using Ambersep 920 and Purolite-A100. Selective molybdenum solutions were regenerated following uranium sorption, initially at pH 2.0, and then raised to 2.5 using ammonia. This pH was chosen since lower pH values (2.0–2.4) produce higher acid concentrations, which diminish anion exchange capacity due to competing acid anions. Furthermore, to reach a pH value above 2.5, significant amounts of ammonia are required. At pH 2.5, polymeric anions such as $Mo_7O_{24}^{6-}$ and $Mo_4O_{13}^{2-}$ and other molybdenum anions, are effectively sorbed.

Detailed analysis of experimental data indicates that anion exchanger Ambersep 920 has a greater sorption capacity, compared to Purolite A100. During the 21-hour (1,260 minutes) sorption process using Ambersep 920, the rate of molybdenum extraction was 88.2% (Figure 11). Raising the process time to 44 hours (1,440 minutes) resulted in only a 0.3% increase in sorption efficiency, indicating that Ambersep 920 became saturated with molybdenum and equilibrium was attained between the anion exchanger and solution. Thus, Ambersep 920 was determined to be the optimal sorbent for molybdenum sorption extraction, and the optimal process time was 1,260 minutes. These findings are consistent with those published in the

literature on molybdenum sorption. For example, Azimov *et al.* [53] investigated the sorption of molybdenum on anion exchangers of polycondensation type and indicated that the degree of molybdenum extraction from an ammonium molybdate solution with a content of 1 g/L Mo and pH 4.5 was attained at the level of 85% with synthesized anionite. Upon comparing our data with the findings of Azimov, it is evident that our research achieved a notably high molybdenum extraction efficiency. Furthermore, the experiments maintained a pH level of 2.5, which effectively reduced the costs associated with the neutralization of leaching solutions. In contrast, Azimov's experiments operated at a pH of 4.5.

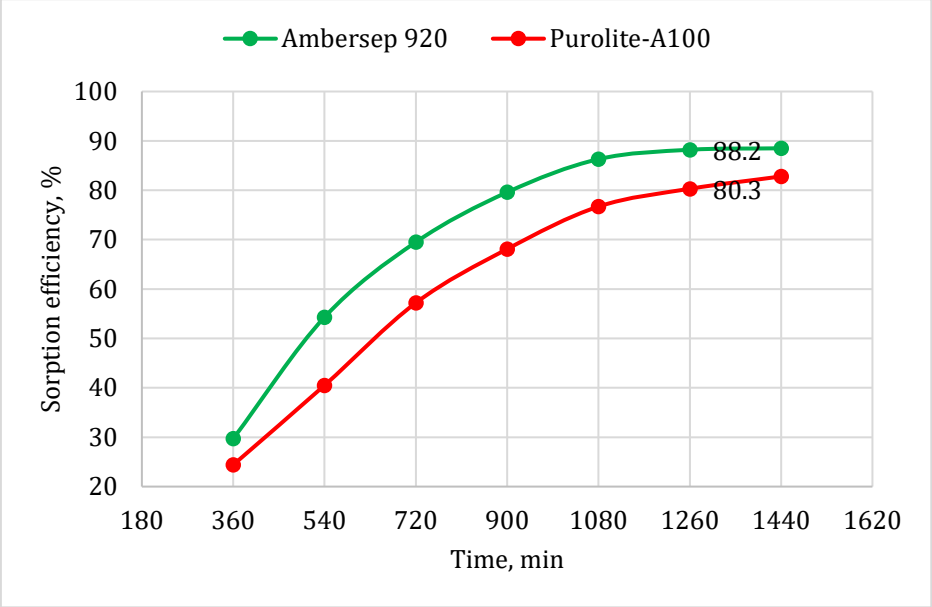



**Figure 11:** Molybdenum sorption efficiency (%) of Ambersep 920 и Purolite-A100 versus reaction time

*Molybdenum Desorption*

As discussed in Experimental Section 4.4.1, serious investigations were conducted to find the optimal circumstances and best desorbing solutions for the desorption of molybdenum. The reagents attempted were ammonia solution (10.0-50 g/L), sodium hydroxide (10-60 g/L), and sulfuric acid solution (100-200 g/L). The study focused on identifying the optimal desorption time and the most effective desorbing solution at optimal concentration. The highest efficiency of molybdenum desorption from anion exchangers was ensured by a 40 g/L solution of sodium hydroxide. Thus, in this study, the data are presented on the process time in the situation when a 40 g/L sodium hydroxide solution was used as the desorbing agent (Table 10).

**Table 10:** Dependence of molybdenum desorption degree on process duration

| Duration of the process, min | Desorption efficiency of molybdenum from Ambersep 920, % | Desorption efficiency of molybdenum from Purolite-A100, % |
|---|---|---|
| 60 | 39.6 | 43.5 |
| 120 | 63.2 | 69.8 |
| 180 | 82.1 | 89.5 |
| 240 | 92.5 | 94.6 |
| 300 | 95.7 | 96.2 |

The data indicate that the efficiency of desorption increases with process time, from 39.6% when the time was 60 minutes to 95.7% when the time was 300 minutes. A closer examination, however,

indicates that a longer time from 240 minutes to 300 minutes contributes only by an additional 3.2% to desorption efficacy. Therefore, to achieve the maximum process and cost economy, a time of 240 minutes was selected. The sulfuric acid solution also resulted in similar desorption results, over 95.0%. However, the use of sulfuric acid results in molybdenum solutions that, when reacted with calcium solutions to give calcium molybdate precipitates, also produce gypsum. Therefore, the best desorbing solution selected was sodium hydroxide.

Time is an important factor in processes of this type, which can follow kinetic models of pseudo-first-order or pseudo-second-order models. According to these models, the desorption rate directly depends on the molybdenum available in the anion exchanger and longer time pushes the process closer to equilibrium, enhancing overall desorption efficiency. Molecules move based on Fick's law of diffusion until concentration equilibrium is reached. With more time, more molybdenum can leave active sites of the anion exchanger, where molybdenum concentration is lower compared to the solution. These mechanisms are confirmed by experiments. For instance, the study [54] confirmed that the rate of desorption rises with time, following a pseudo-second-order model. Study [55] explored how more process time enhances efficiency due to changes in entropy, increasing rates of desorption.

*Calcium Molybdate Precipitation*

Calcium molybdate precipitation was performed according to procedure detailed in Experimental Section, in two steps. Calcium molybdate synthesis at 85 ± 2 °C was implemented in the first step by adding a 40 g/L solution of calcium chloride to desorbate. In the second step, room temperature crystallization of the synthesized calcium molybdate was implemented in the absence of any additional reagent. Temperature control in the two stages was provided with the help of a water jacket equipped with a thermostat. The experiments were primarily designed for the first stage, investigating the completeness of $CaMoO_4$ synthesis from the reaction mixture as a function of process duration.

The data acquired from experiments (Table 11) show that the majority of the calcium molybdate forms in the initial 90 minutes of the synthesis reaction, and an additional 8.0% is produced between 90 and 240 minutes. Chemical kinetics principles, such as the law of mass action, indicate that the rate of a reaction is directly proportional to the concentration of reactants. Higher initial concentrations of reactants hasten the rate of reaction due to more collisions between molybdenum and calcium ions, thereby elevating the prospect of effective collisions for the creation of $CaMoO_4$. These types of collisions have a better likelihood of overcoming the activation energy barrier, thereby promoting precipitation. Investigations into the precipitation of sparingly soluble rare metal compounds, *i.e.,* rhenium, also point out that higher concentrations of ions significantly accelerate the precipitation process.

In a published work on production of calcium molybdate, the researchers obtained a yield of around 78.0% [56], while this research attained a yield of 89.0%. This increased percentage recovery is due to the particular two-stage precipitation procedure of bringing the reaction mixture of the desorbate and calcium chloride solutions quickly to conditions that experience fast cooling to room temperature. Rapid cooling was discovered to enhance the crystal growth rate and overall yield of the product. Based on these findings, the ideal process conditions for the synthesis of calcium molybdate are a period of 240 minutes to obtain the maximum molybdenum extraction. Afterwards, the reaction mixture is poured into another thermostat where precipitation of the calcium molybdate occurs at 25 ± 2 °C for 30 minutes. The resultant product calcium molybdate contains 25.2-27.0% molybdenum.

**Table 11:** Dependence of calcium molybdate formation degree on process duration

| Duration of the process, min | Yield of calcium molybdate, % |
|---|---|
| 30 | 39.6 |
| 60 | 69.5 |
| 90 | 81.2 |
| 120 | 84.4 |
| 180 | 87.2 |
| 240 | 89.0 |

*Vanadium Sorption*

The scrutinization of vanadium sorption followed the methodology outlined in experimental section, aiming to grasp the effect of process duration on vanadium anion sorption, using Ambersep 920 and Purolite-A100. Solutions for vanadium sorption were obtained post-molybdenum sorption, with a pH of 2.5 and an ORP of 380-400 mV. Under these conditions, vanadium exists in oxidation state IV and is not sorbed by the anion exchanger. Therefore, pH and ORP adjustments were made according to the described methodology. The primary focus of the research was to identify the optimal process duration (Figure 12).

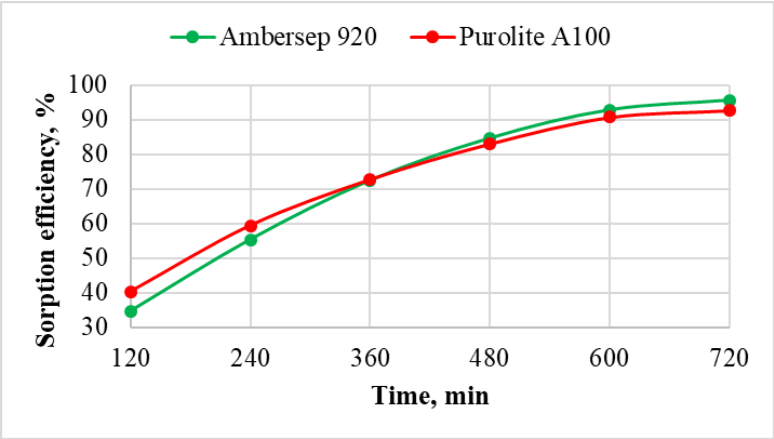



**Figure 12:** Vanadium sorption efficiency (%) of Ambersep 920 and Purolite A100 versus reaction time

Studies indicate that while Ambersep 920 and Purolite A100 anion exchangers exhibit similar sorption properties, their efficiencies vary significantly over different time stages (Figure 12). During the initial 240 minutes of the sorption process, Purolite A100 demonstrates higher sorption capacity, attributable to its faster adsorption kinetics, which are influenced by its surface structure and porosity, facilitating rapid ion capture. Conversely, extending the experiment to 720 minutes illustrates Ambersep 920's superior sorption behaviour, which is likely due to differences in sorption dynamics and mass transfer. This finding is consistent with the literature [57]. The macroporous weak-base resin A100, containing tertiary amine groups, rapidly engages accessible sorption sites and reaches its optimal capacity within 40–50 min, with adsorption isotherms well described by the Langmuir model. The calculated activation energy (25 kJ $mol^{-1}$) indicates a transition from film diffusion to intraparticle diffusion, which accounts for the accelerated uptake at short contact times. Ambersep 920 may possess more stable and long-term sorption sites that are activated at later interaction stages. The surface functional moieties of Ambersep 920 may provide stronger anion interactions that become more effective as the system approaches equilibrium. The sorption capacity difference between these anion exchangers is only 1.4%, underscoring their overall chemical and physical property similarity. Therefore, Purolite A100's short-term advantages are beneficial for

installations requiring rapid effects, while Ambersep 920 ensures higher extraction rates in long-term processes.

Upon completion of the vanadium sorption process, the saturated anion exchangers proceed to the desorption phase.

*Vanadium Desorption*

The vanadium desorption process from saturated anion exchangers was scrutinized using the methodology outlined in Experimental Section. Preliminary experiments aimed at identifying the optimal sodium hydroxide concentration, conducted over 300 minutes, revealed that a 6% concentration is most effective (Table 12).

**Table 12:** Effect of sodium hydroxide concentration on vanadium desorption degree

| NaOH concentration, % | 3 | 6 | 9 | 12 |
|---|---|---|---|---|
| Desorption efficiency of vanadium from Ambersep 920, % | 74.5 | 97.2 | 97.4 | 97.4 |
| Desorption efficiency of vanadium from Purolite-A100, % | 61.2 | 77.6 | 86.8 | 91.7 |

Table 12 demonstrates that sodium hydroxide (NaOH) concentration is crucial in the vanadium desorption process from saturated anion exchangers. A 3.0% NaOH concentration is insufficient for complete vanadium desorption due to the inadequate generation of hydroxide ions ($OH^-$) required to disrupt the bond between vanadium and the anion exchanger. Increasing NaOH level to 6.0% remarkably enhances the desorption efficacy to 97.2%, as the higher concentration provides more $OH^-$ ions, facilitating effective breaking of ionic bonds (*e.g.,* between the quaternary ammonium group ($R_4N^+$) and vanadium anions) and releasing vanadium from the anion exchanger. Further augmentation of NaOH level to 9.0% and 12.0% does not yield significant alterations in desorption efficiency, indicating equilibrium where all accessible ionic bonds are already broken.

Following the determination of optimal desorbing solution concentration, the effect of period on desorption efficiency was scrutinized. The results of these studies are reported in Figure 13.

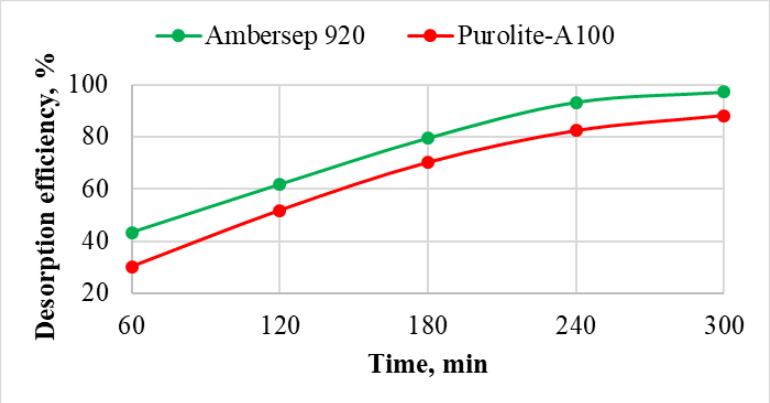



**Figure 13:** Vanadium desorption efficiency (%) from Ambersep 920 and Purolite-A100 versus reaction time

As shown in the experimental data, the use of a 6% NaOH solution as the desorbing agent resulted in a vanadium desorption efficiency of 97.2% from the Ambersep 920 anion exchanger within 300 minutes, compared to 88.2% for the Purolite A100 under identical conditions. This fact is attributable to structural and chemical differences between the two resins. Ambersep 920 possesses a greater density and accessibility of exchange sites, along with a higher availability of functional groups capable of interacting with vanadium anionic species, thereby promoting more efficient desorption. In contrast, Purolite A100 may exhibit a more compact structure or

reduced accessibility of its functional groups, which limits its desorption capacity. These observations are consistent with literature reports showing that V(V) desorption efficiency is strongly influenced by the type of anion exchanger (strong-base vs. weak-base), the concentration of the alkaline eluent, and the contact time. For instance, Jeon *et al.* [58] reported equilibrium vanadium desorption exceeding 90% within approximately 30 minutes using either HCl or NaOH eluents on a porous anion exchange resin, highlighting the inherently high elutability of vanadate species in strong eluents. Similarly, a review by Wołowicz *et al.* [59] systematized desorption performance ranges: Amberlite IRA-400 (SBA-I) achieved 57–72% within 30 minutes using 2 M NaOH; resin 717 reached 81.7% in just 5 minutes; D201 yielded 91.2% using 5% NaOH with 10% NaCl; and WBA resin 2017 exceeded 95% with 3 M NaOH.

The result of 97.2% vanadium desorption from Ambersep 920 using 6% NaOH over an extended 300-minute contact time lies at the upper bound of reported values. This high efficiency can be attributed to the combination of rigid Type II quaternary ammonium functional groups and a macroporous polymer matrix, which together facilitate the reversible exchange of vanadate complexes with hydroxide ions.

*Ammonium Metavanadate Precipitation*

The solutions obtained from vanadium desorption experiments are utilized in the precipitation of ammonium metavanadate. The precipitation experiments were conducted following a methodology similar to that used for calcium molybdate precipitation. In the first stage, termed the “synthesis” stage of ammonium metavanadate, the temperature is maintained at 85 ± 2 °C in thermostated glass reactors for the specified duration. Subsequently, crystallization is performed at 15 ± 2 °C with constant stirring in a separate reactor. During the initial 3.0-4.0 minutes of the first stage, ammonium sulfate solution is added dropwise until the molar ratio of ammonium sulfate to vanadium reaches 3:1, requiring 29.2 mL of ammonium sulfate solution at a concentration of 50 g/L.

**Table 13:** Dependence of ammonium metavanadate formation degree on process duration

| Duration of the process, min | Yield of ammonium metavanadate, % |
|---|---|
| 30 | 52.4 |
| 60 | 71.3 |
| 90 | 84.7 |
| 120 | 98.6 |
| 150 | 98.6 |

The findings reported in Table 13 indicate that the yield of the product when ammonium metavanadate crystallizes from a solution mixture prepared for 30 minutes is 52.4%. Increasing the synthesis time to 120 minutes provides a yield of 98.6% with no additional augmentation obtained beyond this time. Chemical kinetics asserts that the rate of reaction is directly proportional to the concentration of reactants, according to the law of mass action. This rule establishes that the rate of a chemical reaction depends on the concentration of the reactants. A high concentration of the original reactants produces a larger reaction rate and leads to the precipitation of ammonium metavanadate. The precipitate of ammonium metavanadate is obtained in this study with 72.5-74.5% $V_2O_5$ content, which after calcination at 450 °C for 1 hour is converted to vanadium pentoxide with minimum 99.0% $V_2O_5$ content.

*REM Sorption*

To study the selective sorption extraction procedure for rare earth metals (REMs), vanadium sorption solutions with pH in the range 1.6-1.7 were utilized. To facilitate the supply of conditions supportive of the REM sorption on the

cation exchanger, the pH of the solution was adjusted to 2.0 with ammonia solution. Prior to sorption, the solution was analyzed, and a total REM concentration of 0.23 g/L was determined, with individual rare earth metal concentrations (mg/L) of: Gd – 37.19, Ce – 29.41, Y – 57.72, Dy – 26.09, La – 16.26, Yb – 44.23, Sm – 19.10. Sorption was performed using the procedure described in section 4.4.3 with the cation exchanger KU-2-8 H. This cation exchanger was employed because it possesses the best characteristics, *i.e.,* high exchange capacity and osmotic stability, which ensure efficient sorption of REM ions from solutions. KU-2-8 H works well over a wide range of pH and temperature, making it applicable to varied conditions [60]. The experimental results indicate that KU-2-8 H is equivalent in performance (*e.g.,* exchange capacity, osmotic stability, etc.) to analogues such as Dowex HCR-S and Lewatit S-100, but at significantly lower expense. The cost-effectiveness of KU-2-8 H is particularly desirable for industrial use on a large scale. The use of KU-2-8 H in our REM sorption experiments is justified by its efficacy and economic affordability.

One of the objectives of the current research was to determine the minimum duration of the sorption process that allows for maximal sorption of REM ions onto the cation exchanger. The experimental tests were conducted using the aforementioned methodology, with analyses of REM content in the solution performed every 30 minutes after the start of the process. The results of tests for recognizing the optimal duration of the process for the extraction efficiency of the total amount of REMs are presented in Table 14.

**Table 14:** Dependence of REM sorption degree on process duration

| Duration of the process, min | Sorption efficiency, % |
|---|---|
| 30 | 36.2 |
| 60 | 58.5 |
| 90 | 72.3 |
| 120 | 82.8 |
| 150 | 87.8 |
| 180 | 87.9 |

The data illustrate that the sorption dynamics are significantly influenced by the concentration of rare earth metals in the aqueous phase. At relatively high REM concentrations, over 36% of the total REMs are sorbed within the first 30 minutes, equating to approximately 1.2% per minute. As the process duration increases, the sorption rate diminishes; yet, the cation exchangers continue to saturate with REM ions. After 150 minutes, a high sorption efficiency of 87.8% is achieved. This duration is deemed optimal, as extending the process by an additional 30 minutes only enhances REM extraction by 0.3%, indicating a sorption rate of about 0.01% per minute beyond 150 minutes. For a detailed analysis of individual rare earth metal sorption, the post-sorption solution was analyzed using chemical methods. The results of these studies are presented in Table 15.

**Table 15:** Results of experiments on the sorption of REM

| Parameter | REM Concentration / Sorption efficiency | | | | | | | | |
|---|---|---|---|---|---|---|---|---|---|
| | Ce | Y | Dy | La | Yb | Gd | Sm | Σ REM | $Fe_{total}$ |
| REM concentration, mg/L | 29.41 | 57.72 | 26.09 | 16.26 | 44.23 | 37.19 | 19.1 | 230 | 0.350 |
| Sorption efficiency, % | 93.2 | 91.7 | 85.4 | 94.6 | 80.2 | 79.8 | 89.6 | 87.8 | 80.0 |

As indicated in Table 15, the cation exchanger used exhibits high sorption rates for all REMs in the solution, with lanthanum, cerium, yttrium, samarium, and dysprosium being the most effectively sorbed metals. The differences in sorption rates among these rare earth metals are

minimal. To understand this pattern, FTIR spectroscopic studies were conducted on both the initial cation exchanger and the saturated cation exchanger post-sorption. IR spectroscopic analysis helps elucidate the state of REMs within the ion-exchange system and predict their behavior during the sorption process.

The FTIR spectrum of the initial KU-2-8H sorbent in H-form (Figure 14) displays bands corresponding to the styrene-divinylbenzene matrix of the ion exchanger at 3,064; 3,028; 2,923; 2,852; 1,601; 1,496; 1,452; 1,413; 1,183; 834; 775; and 675 $cm^{-1}$. Intense absorption bands at 1,183; 1,128; 1,039; and 1,009 $cm^{-1}$ are indicative of the stretching vibrations of sulfo groups in sulfonic cation exchangers, while bands at 619 and 580 $cm^{-1}$ correspond to the C-S vibrations of sulfo groups.

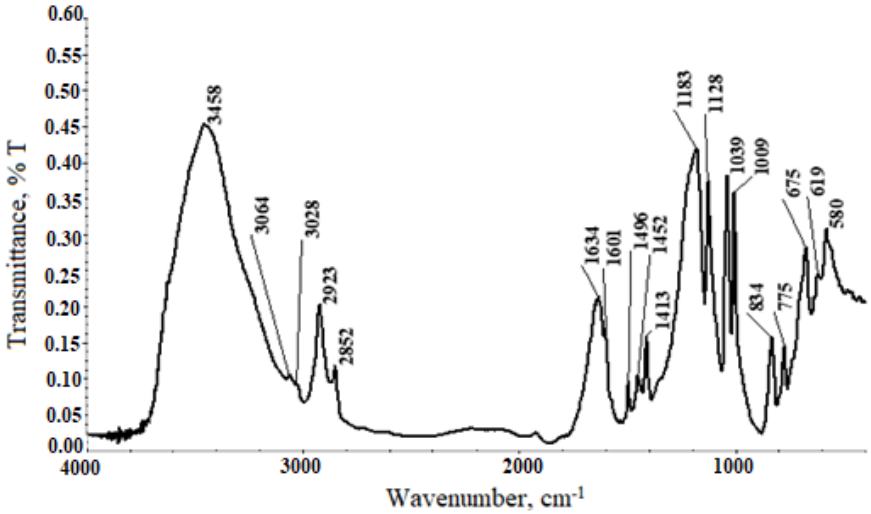



**Figure 14:** FTIR Spectrum of the Initial KU-2-8H Sorbent

As a result of mathematical processing of the cation exchanger spectra in the range of 1,400–900 $cm^{-1}$ (Figure 15), it was found that the intensity of the stretching vibration band of sulfo groups coordinated by rare earth metals at a wavenumber of 1,220 $cm^{-1}$ decreases in the order La (0.138), Ce (0.128), Y (0.126), Sm (0.125), and Dy (0.103). This trend corresponds to the ionic radii of rare earth metals for a coordination number of 12 - La (1.877 Å), Ce (1.825 Å), Y (1.801 Å), Sm (1.802 Å), Dy (1.773 Å) [45].

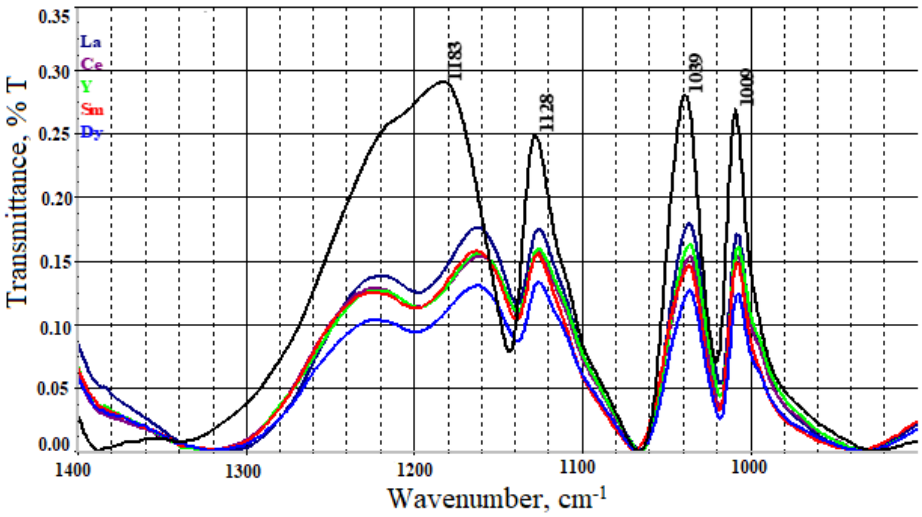



**Figure 15:** FTIR spectra of the ion exchanger saturated with REM

Thus, based on the FTIR spectroscopic scrutiny of the KU-2-8H ion exchanger saturated with rare earth metals, it can be inferred that REM cations interact with the sulfo moieties on ion exchanger in the resin backbone, forming complexes surrounded by water molecules in the inner hydration shell. The size of these complexes influences the sorption degree of individual REMs and is directly dependent on the ionic radius of the complexing agent and its coordination number [61]. The rare earth metals can be ranked by their maximum sorption degree on the KU-2-8H ion exchanger in the following order: La – Ce – Y – Sm – Dy, corroborating the aforementioned dependencies. Therefore, the FTIR spectroscopic analysis results provide insights into how the nature of rare earth metals affects their sorption extraction efficiency.

*REM Desorption*

This section presents the findings of the study on the desorption process of REMs in a static mode. The work was conducted to select the optimal desorbing solution and experimentally determine the optimum period of desorption process. A literature review was performed to select the desorbing solution, and the principal findings are presented below. A group of researchers [62,63] investigated desorption of neodymium from cation sulfonic exchanger KU-2-8H using solutions of sulfuric and nitric acid. According to them, 97.5% neodymium desorption was achieved with 200 g/dm$^3$ sulfuric acid solution, while 40 g/dm$^3$ and 150 g/dm$^3$ resulted in 30.8% and 76.8% desorption, respectively. Sulfuric acid elution can result in REM sulfate precipitates being deposited.

In desorption experiment, sulfuric acid was used at a concentration of 100 g/dm$^3$. The tests were performed statically at a solid-to-liquid ratio of 1:10 following the methodology described in the experimental section. The results are presented in Table 16.

**Table 16:** Effect of process period on the degree of vanadium desorption

| **Duration, min** | 30 | 60 | 90 | 120 | 150 |
|---|---|---|---|---|---|
| Desorption efficiency of REM, % | 41.2 | 67.4 | 82.8 | 91.5 | 93.8 |

The analysis results indicate that the desorbing solution used in the current study exhibits excellent performance for desorption of total REMs, achieving a maximum desorption degree of 93.6% at 150 minutes. The resulting desorption solution, containing 0.189 g/L of total REMs, was subsequently used in the precipitation process to acquire the REM concentrate.

*REM Concentrate Precipitation*

The solutions obtained after the desorption process, containing 0.189 g/L of total REM, were directed to the precipitation process to obtain the REM concentrate. The precipitation studies were conducted following the methodology described in experimental section. The objective was to determine the minimum duration required for the maximum precipitation of rare earth metals as carbonates, occurring through the following reactions:

$2Gd^{3+}+3Na_2CO_3 \rightarrow Gd_2(CO_3)_3+6Na^+$
$2Ce^{3+}+3Na_2CO_3 \rightarrow Ce_2(CO_3)_3+6Na^+$
$2Y^{3+}+3Na_2CO_3 \rightarrow Y_2(CO_3)_3+6Na^+$
$2Dy^{3+}+3Na_2CO_3 \rightarrow Dy_2(CO_3)_3+6Na^+$
$2La^{3+}+3Na_2CO_3 \rightarrow La_2(CO_3)_3+6Na^+$
$2Yb^{3+}+3Na_2CO_3 \rightarrow Yb_2(CO_3)_3+6Na^+$
$2Sm^{3+}+3Na_2CO_3 \rightarrow Sm_2(CO_3)_3+6Na^+$

For the precipitation of the REM concentrate, 1.0 L of the solution obtained post-desorption was utilized. Sodium carbonate was added in an amount three times the stoichiometrically required quantity. Upon dissolving the calculated mass of sodium carbonate (0.55 g), the crystallization process was initiated with continuous stirring. The REM content in the solution was analyzed at 30-minute intervals until the concentration stabilized. The research results are presented in the Table 17.

**Table 17:** Dependence of rare earth metal concentrate yield on process duration

| Duration of the process, min | Yield of REM concentrate, % |
|---|---|
| 30 | 39.3 |
| 60 | 62.6 |
| 90 | 79.7 |
| 120 | 88.6 |
| 150 | 90.8 |
| 180 | 91.2 |

The experiment revealed that during crystallization of REM, the yield of the concentrate during the first 30 minutes was 39.3%. Extending the process duration to 180 minutes increased the yield to 91.2%. However, the yield only increased by 0.4% during the last 30 minutes (150-180 minutes), indicating a slowdown in the crystallization process. Intensive crystallization of REMs is observed in the first 30 minutes due to the high concentration of ions in the solution and a high degree of supersaturation, which provides the maximum rate of crystallization. From 30 to 150 minutes, the crystallization rate gradually declines as the concentration of REM ions in the solution and the degree of supersaturation decrease. Between 150 and 180 minutes, the process of crystallization is nearing its end, and further extension of time does not notably enhance the yield of the product, suggesting a state of equilibrium in which the precipitation and dissolution rates of crystals are equal. Based on the dynamics of REM concentration decrease in the solution and the yield of the concentrate, the optimal process duration is determined to be 180 minutes since the yield increase for the last 30 minutes is only 0.4% and further increase in time becomes impractical. The reactions of REM ions with sodium carbonate are ion-exchange reactions resulting in the production of insoluble rare earth metal carbonates. The REM ions ($R^{3+}$) interact with the carbonate ions ($CO_3^{2-}$) to form insoluble carbonates ($R_2(CO_3)_3$), which precipitate out and allow the REMs to be separated from the solution, yielding the REM concentrate.

The precipitate acquired, a concentrate of rare earth metals (REM), was calcined at 500 °C for one hour and subsequently was brought under analysis. Chemical analysis indicated that the concentrate predominantly consists of iron and aluminum oxides, with an REM content of 5.6%. Electron probe microanalysis of the REM concentrate (Figure 16) affirmed the existence of a significant concentration of REM in the final product.

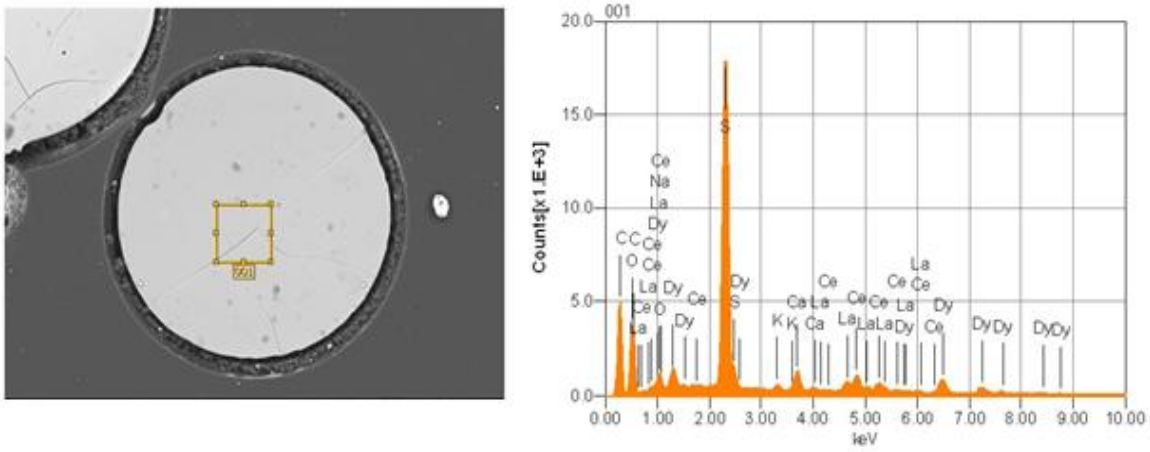



**Figure 16:** Results of electron probe microanalysis of REM concentrate

Several other studies have confirmed the high efficiency of carbonate-based desorption of REMs under optimized conditions. For example, in the work of Wang *et al.* [64], ammonium bicarbonate

($NH_4HCO_3$) was employed for the precipitation of REM carbonates from a concentrated sulfate solution containing Ce, Gd, and Y. Under conditions of a final pH of 6.8, temperature of 25 °C, $NH_4HCO_3$ concentration of 0.6 mol $L^{-1}$, feed rate of 0.5 mL $min^{-1}$, seed crystal dosage of 7.5 %, and stirring speed of 300 rpm, a precipitation efficiency of 99.78 % was achieved, with a rare earth oxide content of 57.69 %. Another study by Silva *et al.* [65] compared the precipitation of rare earth elements as carbonates and oxalates from a purified sulfuric solution. Oxalate precipitation yielded >96 % recovery with high rare earth oxide purity (99.2 %), while carbonate precipitation at 60 °C also resulted in REM recovery efficiencies exceeding 96 %, but the rare earth oxide purity was lower (68.5 %) due to a higher proportion of co-precipitated impurities.

## Conclusion

The present work puts forward a breakthrough advance in the metallurgical processing of black shale ores by elucidating intrinsic limitations of direct acid leaching and introducing a novel low-temperature sintering technology using ammonium hydrosulfate at 350 °C. The new technology triumphantly overcomes the encapsulation of uranium, vanadium, molybdenum, and rare earth metals in strong carbon-silica matrices and enables their efficient transformation into soluble species, thereby raising extraction yields remarkably. By operating at substantially lower temperatures, compared to conventional pyrometallurgical methods, the process not only reduces energy consumption and operational costs, but also minimizes environmental footprints associated with high-temperature treatments. Systematic optimization of leaching, sorption, and desorption conditions- particularly through precise redox potential and pH control-has made it possible to extract selectively and efficiently target metals with their separation in acceptable ionic states. The development of low-cost methods for vanadium and molybdenum concentrate production further confirms the economic appeal of the process. The coupling of carbon flotation enrichment achieves the fullest exploitation of all of the ore components, offering a closed-loop, resource-saving concept. Cumulatively, these findings form a solid basis for the economically feasible and sustainable extraction of critical metals from black shale ores, providing a blueprint for guiding future resource exploitation strategies in the metallurgical industries.

## Disclosure Statement

The authors declared that they had no known competing financial interests or personal relationships that could have appeared to influence the work reported in this study.

## Funding

This research was funded by the Science Committee of the Ministry of Science and Higher Education of the Republic of Kazakhstan (grant No. BR21881939).

## Authors' Contributions

T. Chepushtanova: Data curation, project administration; S. Yulussov: resources; O. Baigenzhenov: validation, writing – review and editing; A. Khabiev: investigation, visualization; K. Rysbekov: formal analysis; N. Nosbi: writing – original draft; M. Barmenshinova: software; N.N. Yusof: writing – original draft; Y. Merkibaev: methodology, investigation; A. Hosseini-Bandegharaei: validation, writing – review and editing.

## Data availability

All data generated or analyzed during this study are included in this published article.

## ORCID

*Norlin Nosbi*
*https://orcid.org/0000-0002-6531-3476*
*Nur Nabihah Yusof*
*https://orcid.org/0000-0002-1427-0269*
*Ahmad Hosseini-Bandegharaei*
*https://orcid.org/0000-0002-1280-479X*

## References


[1] Wang, W., Chen, J., Feng, X., Ge, X., Zhang, Y., Liang, J., Xu, L. Sedimentary environment and organic matter enrichment mechanism of the silurian gaojiabian black shales in the lower yangtze region, South China. *Minerals*, **2025**, 15(3), 204.

[2] Rais, S., Kembayev, M., Bulegenov, K. Geology and prospects of the Shu-Ile Belt Granitoids as building materials (South Kazakhstan). *International Multidisciplinary Scientific GeoConference: SGEM*, **2023**, 23(1.1), 43-48.

[3] Kenzhaliyev, B., Surkova, T.Y., Azlan, M., Yulusov, S., Sukurov, B., Yessimova, D. Black shale ore of Big Karatau is a raw material source of rare and rare earth elements. *Hydrometallurgy*, **2021**, 205, 105733.

[4] Vind, J., Tamm, K. Review of the extraction of key metallic values from black shales in relation to their geological and mineralogical properties. *Minerals Engineering*, **2021**, 174, 107271.

[5] Li, K., Huang, J., Zhang, Y., Hu, P., Li, S., Xiang, S. Comprehensive extraction of V, Ni and Mo from black shale via selective leaching oxidation process. *Journal of Environmental Chemical Engineering*, **2024**, 12(6), 114581.

[6] Bai, Z., Han, Y., Jin, J., Sun, Y., Zhou, Z. Extraction of vanadium from black shale by novel two-step fluidized roasting process. *Powder Technology*, **2022**, 408, 117745.

[7] Zheng, Q., Zhang, Y., Xue, N. Enhancing effect of vanadium releasing efficiently from lattice in black shale by thermal activation. *Colloids and Surfaces A: Physicochemical and Engineering Aspects*, **2022**, 651, 129773.

[8] Zhou, Z., Zhu, Y., Jin, J., Han, Y., Bai, Z., Tang, Z. Enhanced vanadium extraction from Muscovite-type Vanadium-bearing shale by suspension oxidation roasting pretreatment-acid leaching. *Separation and Purification Technology*, **2023**, 309, 123066.

[9] Kamalesh, A.K., Chernyshova, I.V., Slabov, V., Lode, S., Eccles, R., Ponnurangam, S. Comparison of microwave and conventional roasting in the leaching of rare earth elements, V, Ni, and Li from polymetallic black shale. *Transactions of the Indian Institute of Metals*, **2024**, 77(12), 4367-4382.

[10] Aleksandrova, T., Nikolaeva, N., Afanasova, A., Romashev, A., Aburova, V., Prokhorova, E. Extraction of low-dimensional structures of noble and rare metals from carbonaceous ores using low-temperature and energy impacts at succeeding stages of raw material transformation. *Minerals*, **2023**, 13(1), 84.

[11] Wu, T., Yang, R., Gao, L., Li, J., Gao, J. Origin and enrichment of vanadium in the Lower Cambrian black shales, South China. *ACS omega*, **2021**, 6(41), 26870-26879.

[12] Schovsbo, N.H. Uranium enrichment shorewards in black shales: A case study from the Scandinavian Alum Shale. *Gff*, **2002**, 124(2), 107-115.

[13] Li, M., Wei, C., Fan, G., Wu, H., Li, C., Li, X. Acid leaching of black shale for the extraction of vanadium. *International Journal of Mineral Processing*, **2010**, 95(1-4), 62-67.

[14] Chang, W., Gang, F. Recovery of vanadium from black shale. *Transactions of Nonferrous Metals Society of China*, **2010**, 20, s127-s131.

[15] Zheng, Q., Zhang, Y., Liu, T., Huang, J., Xue, N. Vanadium extraction from black shale: Enhanced leaching due to fluoride addition. *Hydrometallurgy*, **2019**, 187, 141-148.

[16] Tang, Y., Ye, G., Zuo, Q. Vanadium extraction from the flotation concentrate of vanadium-bearing shale by process of non-roasting enhanced acid leaching and thermodynamics. *Molecules*, **2023**, 28(6), 2706.

[17] Komekova, N., Kozlov, V., Smirnov, K., Shayakhmetova, R., Nesterov, K. Autoclave leaching of vanadium from black shale. *Metallurgist*, **2017**, 60(11), 1186-1190.

[18] Tian, L., Xu, Z., Chen, L., Liu, Y., Zhang, T.A. Effect of microwave heating on the pressure leaching of vanadium from converter slag. *Hydrometallurgy*, **2019**, 184, 45-54.

[19] Li, M., Wei, C., Fan, G., Li, C., Deng, Z., Li, X. Extraction of vanadium from black shale using pressure acid leaching. *Hydrometallurgy*, **2009**, 98(3-4), 308-313.

[20] Baigenzhenov, O., Yulussov, S., Khabiyev, A., Sydykanov, M., Akbarov, M. Investigation of the leaching process of rare-earth metals from the black shale ores of greater karatau. *Kompleksnoe Ispolzovanie Mineralnogo Syra= Complex use of Mineral Resources*, **2019**, 310(3), 76-80.

[21] Baigenzhenov, O., Khabiyev, A., Mishra, B., Turan, M.D., Akbarov, M., Chepushtanova, T. Uranium (VI) recovery from black shale leaching solutions using ion exchange: Kinetics and equilibrium studies. *Minerals*, **2020**, 10(8), 689.

[22] Sahoo, S.K., Kumar, M., Karak, S.K. Fundamentals of metallurgical thermodynamics. *Springer*, 2024, 978-981.

[23] Bejan, A., Tsatsaronis, G. Purpose in thermodynamics. *Energies*, **2021**, 14(2), 408.

[24] Huang, J., Zhang, Y., Huang, J., Liu, T., Cai, Z., Xue, N. Selective leaching of vanadium from roasted stone

coal by dilute sulfuric acid dephosphorization-two-stage pressure acid leaching. *Minerals*, **2016**, 6(3), 75.
[25] Cai, Z., Zhang, Y., Liu, T., Huang, J. Mechanisms of vanadium recovery from stone coal by novel $BaCO_3$/CaO composite additive roasting and acid leaching technology. *Minerals*, **2016**, 6(2), 26.
[26] Zhu, X., Yang, S., Zhou, Z., Jin, J., Han, Y. A sustainable method for high-efficient exploitation of low-grade vanadium-bearing shale ore by oxidation roasting pretreatment. *Journal of Cleaner Production*, **2024**, 447, 141627.
[27] Kamalesh, A.K., Chernyshova, I.V., Slabov, V., Lode, S., Eccles, R., Ponnurangam, S. Comparison of microwave and conventional roasting in the leaching of rare earth elements, V, Ni, and Li from polymetallic black shale. *Transactions of the Indian Institute of Metals*, **2024**, 77(12), 4367-4382.
[28] Tong, Z., Hu, X., Wen, H. Effect of roasting activation of rare earth molten salt slag on extraction of rare earth, lithium and fluorine. *Journal of Rare Earths*, **2023**, 41(2), 300-308.
[29] Baigenzhenov, O., Chepushtanova, T., Altmyshbayeva, A.Z., Temirgali, I., Maldybayev, G., Sharipov, R., Dagubayeva, A. Investigation of thermodynamic and kinetic regularities of asbestos waste leaching processes. *Results in Engineering*, **2024**, 21, 102000.
[30] Li, H., Wang, J., Hou, W., Li, M., Cheng, B., Feng, Y., Xu, T. The study of carbon recovery from electrolysis aluminum carbon dust by froth flotation. *Metals*, **2021**, 11(1), 145.
[31] Bektenov, N., Sadykov, K., Baidullayeva, A., Chinibayeva, N., Chalov, T., Koszhanova, G., Kambarova, E. Vermiculite modified with glycidyl methacrylate, acrylonitrile, and phosphoric acid for the adsorption of molybdenum and rhenium ions from aqueous solutions. *Processes*, **2025**, 13(5), 1584.
[32] Karimova, L., Kairalapov, Y., Tussupbekova, T., Oleinikova, T., Makasheva, G. Hydrometallurgical processing of molybdenum middlings from Shatyrkul-Zhaysan cluster ore. *Journal of Mining and Metallurgy, Section B: Metallurgy*, **2024**, 60(1), 71-83.
[33] Huang, Z., Chen, T., Zhou, Y., Xu, W., Lin, H., Yan, B. Optimization of oxidative leaching for vanadium extraction from low-grade stone coal using response surface methodology. *Processes*, **2020**, 8(12), 1534.
[34] Shevko, V., Aitkulov, D., Badikova, A. Comprehensive processing of vanadium-containing black shale tailings. *Periodica Polytechnica Chemical Engineering*, **2022**, 66(4), 617-628.
[35] Dzhumankulova, S., Zhuchkov, V., Alybaev, Z.A., Bekenova, G. Review of state and prospects for development of vanadium production in the Kazakhstan Republic. *Metallurgist*, **2020**, 64(1), 75-81.
[36] Jin, J., Yu, X., Bai, Z., Zhou, Z., Han, Y., Li, Y. The effect and mechanism analysis of calcium and magnesium between the blank roasting-leaching process of vanadium shale. *Fuel*, **2025**, 396, 135320.
[37] Bai, Z., Sun, Y., Xu, X., Jin, J., Han, Y. A novel process of gradient oxidation roasting-acid leaching for vanadium extraction from stone coal. *Advanced Powder Technology*, **2024**, 35(1), 104296.
[38] Li, X., Wei, C., Deng, Z., Li, C., Fan, G., Li, M., Huang, H. Recovery of vanadium from $H_2SO_4$-HF acidic leaching solution of black shale by solvent extraction and precipitation. *Metals*, **2016**, 6(3), 63.
[39] Li, M., Wei, C., Zhou, X., Qiu, S., Deng, Z., Li, X. Kinetics of vanadium leaching from black shale in non-oxidative conditions. *Mineral Processing and Extractive Metallurgy*, **2012**, 121(1), 40-47.
[40] Chen, L., Wang, Z., Qin, Z., Zhang, G., Yue, H., Liang, B., Luo, D. Investigation of the selective oxidation roasting of vanadium-iron spinel. *Powder Technology*, **2021**, 387, 434-443.
[41] Zhou, Z., Jin, J., Zhu, Y., Han, Y., Bai, Z., Tang, Z. Effect of roasting temperature on vanadium extraction, kinetics, phase transformation, and microstructure evolution of vanadium-bearing shale during suspension oxidation roasting process. *Advanced Powder Technology*, **2023**, 34(11), 104233.
[42] Kloprogge, J. Interactions of the kaolin minerals with complex organic molecules. In *Spectroscopic Methods in the Study of Kaolin Minerals and Their Modifications*, **2018**, 321-415.
[43] Khabiyev, A., Baigenzhenov, O., Yulussov, S., Akbarov, M., Sydykanov, M. Study of leaching processes of sintered black shale ore. *Kompleksnoe Ispolzovanie Mineralnogo Syra= Complex use of Mineral Resources*, **2020**, 315(4), 5-10.
[44] Shayakhmetova, R., Mukhametzhanova, A., Akbayeva, D., Terlikbaeva, A.Z., Osipov, P., Alimzhanova, A., Zharmenov, A. Magnesium and silicon recovery from chrysotile asbestos waste of the deposit Zhitikara, Kazakhstan. *Scientific Reports*, **2024**, 14(1), 31866.
[45] Binnemans, K., Jones, P.T., Blanpain, B., Van Gerven, T., Pontikes, Y. Towards zero-waste valorisation of rare-earth-containing industrial process residues: a critical review. *Journal of Cleaner Production*, **2015**, 99, 17-38.
[46] Kenzhaliyev, B., Surkova, T., Berkinbayeva, A., Baltabekova, Z., Smailov, K., Abikak, Y., Dosymbaeva, Z. Innovative methods for intensifying the processing of Zinc clinker: Synergy of microwave treatment and ultrasonic leaching. *Metals*, **2025**, 15(3), 246.

[47] Chang, W., Gang, F., Cun-xiong, L., Zhi-gan, D., Xin-bin, L. Pressure acid leaching of black shale for extraction of vanadium. *Transactions of Nonferrous Metals Society of China*, **2010**, 20, s112-s117.
[48] Zharmenov, A., Yefremova, S., Sukharnikov, Y., Bunchuk, L., Kablanbekov, A., Anarbekov, K., Yessengarayev, Y. Carbonaceous materials from rice husk: Production and application in industry and agriculture. *Inżynieria Mineralna*, **2018**, 19(1), 263-274.
[49] Yefremova, S., Sukharnikov, Y.I., Sarsembayeva, N., Kablanbekov, A., Bogdanovich, N., Murtazayeva, D., Zharmenov, A. Carbon and mineral feed additive produced from rice husk. In *Land Reclamation in Ecological Fragile Areas*, **2017**, 511-516.
[50] Liu, Y., Liu, J., Dou, H. Effects of carbon emission on the environment of high-speed vehicles on highways for intelligent transportation systems. *Mobile Information Systems*, **2022**, 2022(1), 3156759.
[51] Li, N., Gao, L., Chattopadhyay, K. Experimental study on the collecting agent for spent potlining flotation index optimization. In *Light Metals 2020*, 1243-1250.
[52] Lee, S., Gibson, C.E., Ghahreman, A. The separation of carbonaceous matter from refractory gold ore using multi-stage flotation: A case study. *Minerals*, **2021**, 11(12), 1430.
[53] Azimov, D., Turabjanov, S., Nazirova, R., Igitov, F., Pulatov, K., Tursunov, D. Investigation of the sorption of molybdenum by anion exchanger of the polycondensation type. In *AIP Conference Proceedings*, **2022**, 2432, 050060.
[54] Lian, J., Zhou, F., Chen, B., Yang, M., Wang, S., Liu, Z., Niu, S. Enhanced adsorption of molybdenum (VI) onto drinking water treatment residues modified by thermal treatment and acid activation. *Journal of Cleaner Production*, **2020**, 244, 118719.
[55] Knopf, D.A., Ammann, M. Adsorption and desorption equilibria from statistical thermodynamics and rates from transition state theory. *Atmospheric Chemistry and Physics*, **2021**, 21(20), 15725-15753.
[56] Latypova, S.S., Eseva, E., Sinikova, N., Akopyan, A. Molybdate-based catalytic systems for aerobic oxidation of organic substrates (a review). *Petroleum Chemistry*, **2023**, 63(11), 1274-1291.
[57] Ultarakova, A., Karshyga, Z., Lokhova, N., Yessengaziyev, A., Kassymzhanov, K., Mukangaliyeva, A. Studies of niobium sorption from chloride Solutions with the Use of Anion-Exchange Resins. *Processes*, **2023**, 11(4), 1288.
[58] Jeon, J.H., Sola, A.B.C., Lee, J.Y., Koduru, J.R., Jyothi, R.K. Separation of vanadium and tungsten from synthetic and spent catalyst leach solutions using an ion-exchange resin. *RSC Advances*, **2022**, 12(6), 3635-3645.
[59] Wołowicz, A., Hubicki, Z. Vanadium (V) removal from aqueous solutions and real wastewaters onto anion exchangers and Lewatit AF5. *Molecules*, **2022**, 27(17), 5432.
[60] Talkybek, J., Kabzhalelov, K., Malimbayeva, Z., Korganbayeva, Z. Features of selective sorption of neodymium and praseodymium ions by interpolymer systems based on industrial sorbents KU-2-8 and AV-17-8. *Polymers*, **2025**, 17(4), 440.
[61] Abdulvaliyev, R., Ultarakova, A., Mukangaliyeva, A., Lokhova, N., Kassymzhanov, K. Comparative analysis of acid leaching for the efficient recovery of lanthanum and cerium from phosphate. *Separations*, **2024**, 11(10), 288.
[62] Jumadilov, T., Kabzhalelov, K. Features of extraction of neodymium ions by interpolymer systems based on salt forms of industrial ionites. *Kompleksnoe Ispolzovanie Mineralnogo Syra= Complex use of Mineral Resources*, **2026**, 336(1), 30-38.
[63] Kenzhaliyev, B., Surkova, T.Y., Yessimova, D. Concentration of rare-earth elements by sorption from sulphate solutions. *Kompleksnoe Ispol'zovanie Mineral'nogo syr'â= Complex Use of Mineral Resources*, **2019**, 310(3), 5-9.
[64] Wang, Q., Qi, T., Yu, H., Zhang, L., Sun, D., Liu, Y., Huang, L. Precipitating rare earth by $NH_4HCO_3$ from a concentrated rare earth and magnesium sulfate solution. *Minerals*, **2025**, 15(5), 525.
[65] Silva, R.G., Morais, C.A., Teixeira, L.V., Oliveira, É.D. Selective precipitation of high-quality rare earth oxalates or carbonates from a purified sulfuric liquor containing soluble impurities. *Mining, Metallurgy & Exploration*, **2019**, 36(5), 967-977.

**HOW TO CITE THIS ARTICLE**
T. Chepushtanova, S. Yulussov, O. Baigenzhenov, A. Khabiev, K. Rysbekov, N. Nosbi, M. Barmenshinova, N.N. Yusof, Y.Merkibaev, A. Hosseini-Bandegharaei, An Innovative Method for Complex Processing of Black Shale Ores to Produce Uranium, Vanadium, Molybdenum, and Rare Earth Concentrates. *Chem. Methodol.*, 2026, 10(1) 75-111
**DOI**: https://doi.org/10.48309/chemm.2026.535012.1988
**URL**: https://www.chemmethod.com/article_231747.html